# Appendix A.3:

# Rawhiti Domain – VsVp 57188

## Table 1: Site Description for Rawhiti Domain ($V_SV_P$ 57188).

| Attribute | Yes/No | | | Description/Date | Symbol in Figure 1 |
|---|---|---|---|---|---|
| | 10-m Buffer | 20-m Buffer | 50-m Buffer | | |
| Near a body of surface water or other free-face features? | No | No | No | The center of the site is approximately 190 meters away from the Avon River. The direction of the free face is roughly NW-SE, while its height is 1-2 meters. | NA |
| Lateral spreading observed during the CES? | No | No | No | Ground cracks indicating lateral spreading were not observed by the mapping team.[1] | NA |
| Nearby buildings or structures? | No | No | Yes | Several residential buildings are situated in the S portion of the 50-m buffer and cover 3% of its area. | White Fill + Brown Outline |
| Sloping land? | No | No | No | NA | NA |
| Step changes in the ground surface? | No | No | No | NA | NA |
| Retaining walls? | No | No | No | NA | NA |
| Vegetation? | Yes | Yes | Yes | Trees cover 6% of the 10-m buffer, 30% of the 20-m buffer, and 45% of the 50-m buffer. They are located in the NW quadrant of the 10-m buffer, the SW, NW, and NE portions of the 20-m buffer, and the N portion and near the SW and SE rims of the 50-m buffer. | White Fill + Green Outline |
| Anthropogenic changes to the site between the LiDAR surveys? | No | No | Yes | Removal of a dwelling close to the SW quadrant of the 50-m buffer between Sep 2014 and Jan 2015 and addition of two new structures on the same property between Jan 2015 and June 2015. | Removed Dwelling: Brown X Sign; Added Structures: Yellow + Sign |
| Other important factors? | No | Yes | Yes | Four concrete patches (covering a total area of 25 $m^2$) are located within the three buffers. Busy two-way road occupies 15% of the 50-m buffer and stretches throughout the NW, SW, and SE quadrants. | Concrete Patches: Purple Outline Road: White Fill + Gray Outline |

Notes: Buffer is the area within a circle of a specified radius with VsVp investigations done at its center (172.721404, -43.506685); Vehicles were occasionally parked on the site, as can be seen for the Feb 2012 LiDAR survey (Figure 55), for which the corresponding LiDAR points were excluded from the settlement analysis.

[1] Canterbury Geotechnical Database. (2012). "Observed Ground Crack Locations", Map Layer CGD0400 - 23 July 2012, retrieved July 09, 2018 from https://canterburygeotechnicaldatabase.projectorbit.com/


**Figure 1: Site plan with areas where LiDAR survey data is considered.**

**Note 1:** The area selected for settlement assessment (Patch A) is free of vegetation, structures, anthropogenic changes, and other important factors that have the potential to influence LiDAR measurements.

**Table 2: LiDAR flight error adjustments, global adjustments for the difference between average LiDAR point elevations and benchmark survey elevations, and vertical tectonic movement adjustments.**

| | Adjustments (mm) | | |
|---|---|---|---|
| Earthquake Event(s) | LiDAR Flight Error | Global Offset[2] | Tectonic Vertical Movement |
| Sep-10 | 0 | -3 | 0 |
| Feb-11 | 0 | 16 | -20 |
| Jun-11 | 0 | 38 | -50 |
| Dec-11 | 0 | -65 | 20 |
| CES | 0 | -14 | -50 |
| Any LiDAR survey affected by ejecta? | | | No |

Note: The negative sign indicates the subtraction from the ground surface subsidence, while the positive sign indicates the addition to the ground surface subsidence.

**Table 3: LiDAR Measurement Error.**

| Surveys | Buffer | Area Averaged Difference Indicating Repeat Measurement Error (mm) | $\sigma^*_{\text{individual LiDAR points}}$ (mm) | %Reduction in $\sigma$ due to Area Averaging of LiDAR Points |
|---|---|---|---|---|
| Post Feb 2011: Mar 2011 and May 2011 | 10-m | 56 | 59 | [88, 95] |
| | 20-m | 52 | | |
| | 50-m | 53 | | |
| Post Dec 2011: Feb 2012 and Oct 2015 | 10-m | 22 | 70 | [31,31] |
| | 20-m | 22 | | |
| | 50-m | 21 | | |

*Standard deviation.

**Table 4: Ground surface subsidence adjustments due to LiDAR measurement error.**

| Earthquake Event(s) | $\sigma_{\text{pre-EQ LiDAR survey}}$ (mm) | $\sigma_{\text{post-EQ LiDAR survey}}$ (mm) | $\sigma_{\text{total}}$ (mm) | Area Average Adjusted $\sigma$ (mm) ** |
|---|---|---|---|---|
| Sep-10 | 158 | 56 | 134 | ±127 |
| Feb-11 | 56 | 59 | 59 | ±56 |
| Jun-11 | 59 | 61 | 62 | ±59 |
| Dec-11 | 61 | 70 | 87 | ±82 |
| CES | 158 | 70 | 124 | ±118 |

**Based on the highest %Reduction in Table 3.

[2] Russell, J., & van Ballegooy, S. (2015). *Canterbury Earthquake Sequence: Increased liquefaction vulnerability assessment methodology*. New Zealand: Tonkin & Taylor Ltd.

**Table 5: Raw liquefaction-related ground surface subsidence using original LiDAR points.**

| | Average Ground Surface Subsidence (mm) | | |
|---|---|---|---|
| Earthquake Event(s) | 10-m Buffer | 20-m Buffer | 50-m Buffer |
| Sep-10 | 36 | 26 | 35 |
| Feb-11 | 88 | 85 | 85 |
| Jun-11 | 33 | 24 | 20 |
| Dec-11 | 20 | 24 | 25 |
| CES | 177 | 159 | 164 |

**Table 6: Corrected liquefaction-related ground surface subsidence using original LiDAR points with the calculated adjustments in Table 2.**

| | Average Calculated Ground Surface Subsidence (mm) | | |
|---|---|---|---|
| Earthquake Event(s) | 10-m Buffer | 20-m Buffer | 50-m Buffer |
| Sep-10 | 33 ± 125 | 23 ± 125 | 32 ± 125 |
| Feb-11 | 84 ± 50 | 81 ± 50 | 81 ± 50 |
| Jun-11 | 21 ± 50 | 12 ± 50 | 8 ± 50 |
| Dec-11 | -25 ± 75 | -21 ± 75 | -21 ± 75 |
| CES | 113 ± 125 | 95 ± 125 | 100 ± 125 |

Notes: Plus/minus values are same as those in Table 4, but rounded to the nearest 25; Positive overall values indicate ground surface subsidence, while negative overall values indicate ground surface uplift.

**Table 7: Corrected liquefaction-related ground surface subsidence using LiDAR DEMs.**

| | Estimated Ground Surface Subsidence (mm) | | | | | | | | |
|---|---|---|---|---|---|---|---|---|---|
| | 10-m Buffer | | | 20-m Buffer | | | 50-m Buffer | | |
| Earthquake Event(s) | 16th %ile | 50th %ile | 84th %ile | 16th %ile | 50th %ile | 84th %ile | 16th %ile | 50th %ile | 84th %ile |
| Sep-10 | 50 | 50 | 50 | 50 | 50 | 50 | 50 | 50 | 50 |
| Feb-11 | 50 | 50 | 150 | 50 | 50 | 150 | 50 | 50 | 150 |
| Jun-11 | 50 | 50 | 50 | 50 | 50 | 50 | 50 | 50 | 50 |
| Dec-11 | 50 | 50 | 50 | 50 | 50 | 50 | 50 | 50 | 50 |
| CES | 150 | 150 | 150 | 150 | 150 | 150 | 150 | 150 | 150 |

Note: These percentiles are not the exact statistical measures; they indicate the spatial variability of ground surface subsidence.

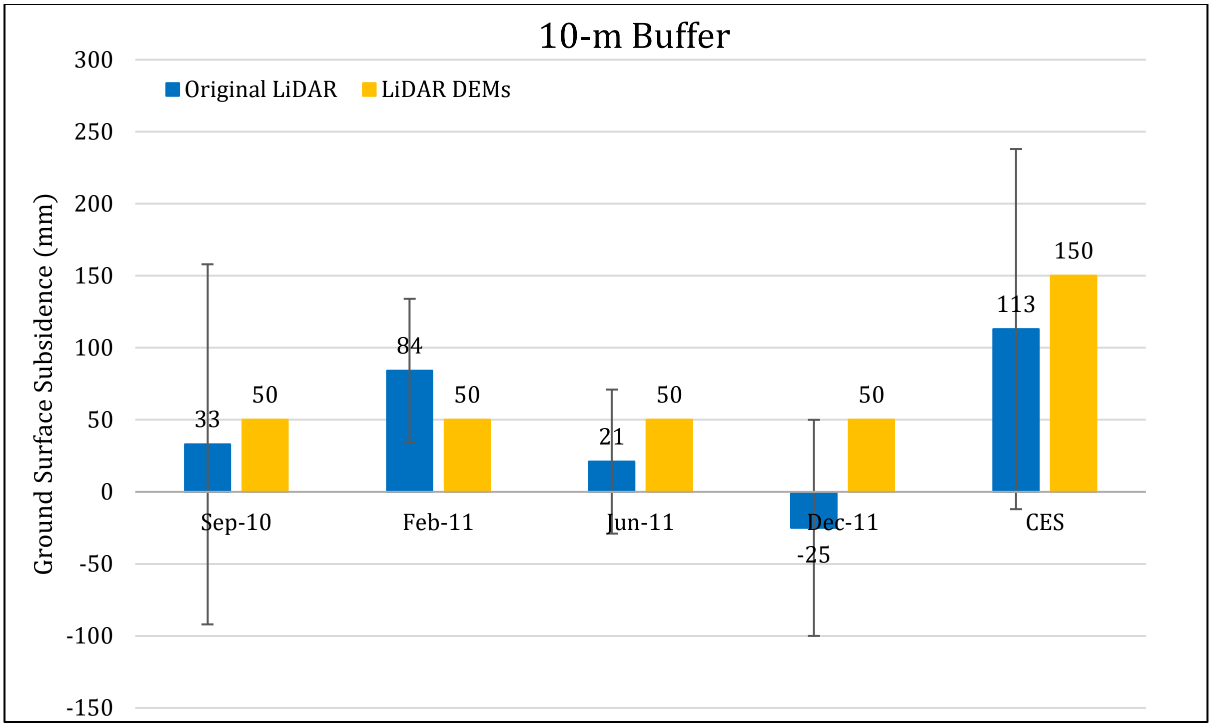


**Figure 2: Comparison between ground surface subsidence determined from original LiDAR survey points and ground surface subsidence (50th %ile) estimated using LiDAR DEMs for the 10-m buffer.**

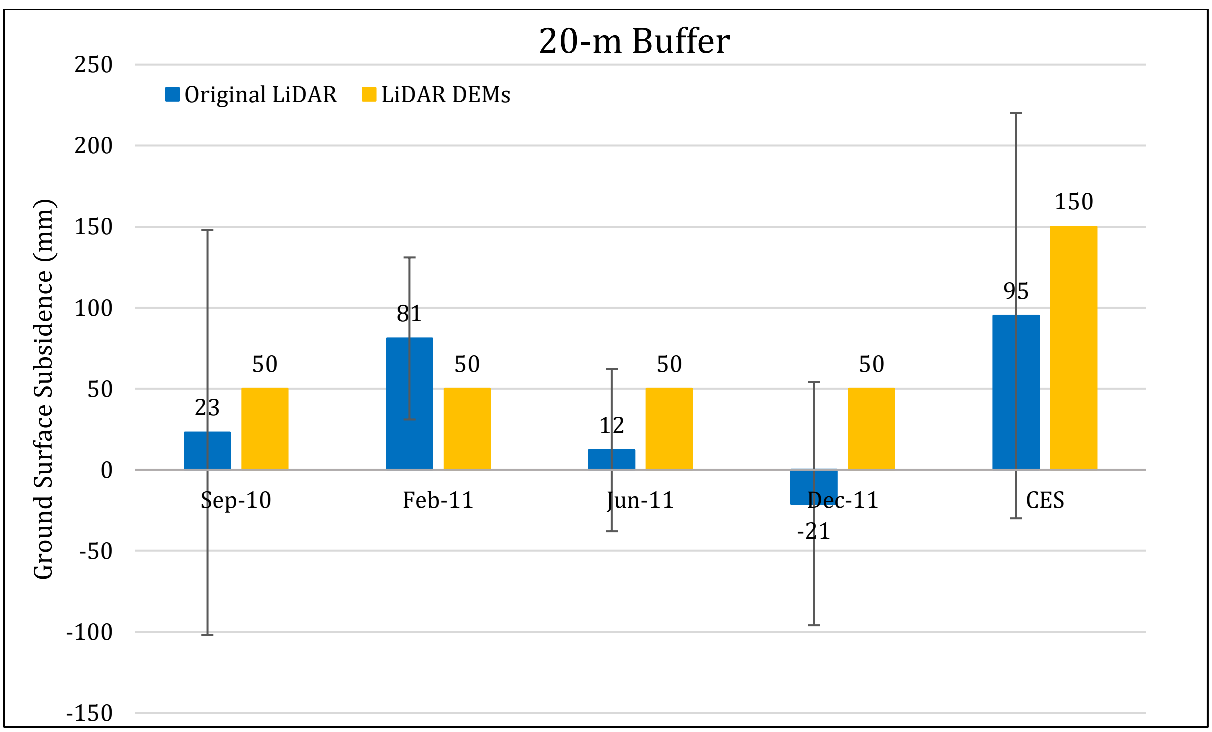


**Figure 3: Comparison between ground surface subsidence determined from original LiDAR survey points and ground surface subsidence (50th %ile) estimated using LiDAR DEMs for the 20-m buffer.**

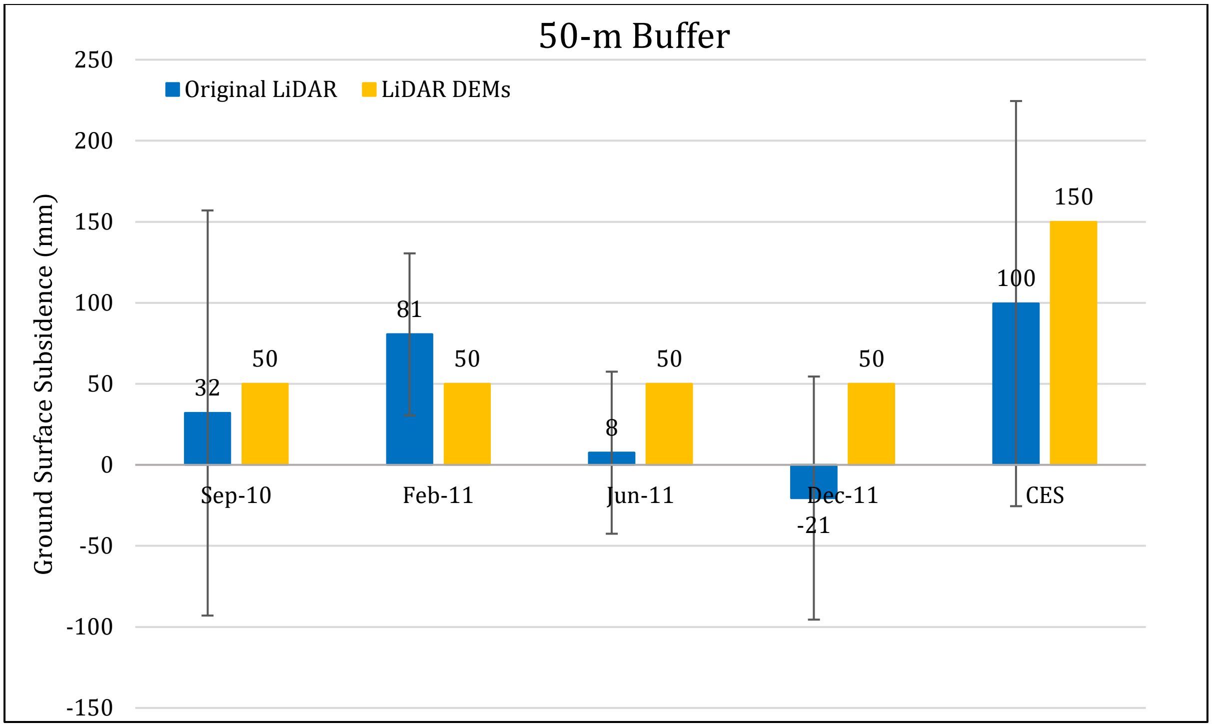


**Figure 4: Comparison between ground surface subsidence determined from original LiDAR survey points and ground surface subsidence (50th %ile) estimated using LiDAR DEMs for the 50-m buffer.**

**Note 2:** The ground surface subsidence values determined from original LiDAR survey points are similar to the ground surface subsidence values estimated using LiDAR DEMs for all earthquake events.

**Table 8a: Ejecta-Induced settlement for the top 20 m of the soil profile for the 10-m buffer for the 50th %ile PGA, $P_L$=50%, and $C_{FC}$=0.13 using BI-2014, ZRB-2002, and $I_C$ cutoff of 2.6.**

| Earthquake Event(s) | $M_W$ | PGA (g) | Depth to Groundwater (m) | $S_T$(mm) | $S_{V1D}$ (mm) | $S_{E,L}$ (mm) |
|---|---|---|---|---|---|---|
| Sep-10 | 7.1 | 0.18 | 1.5 | 33±125 | 1±20 | 32±127 |
| Feb-11 | 6.2 | 0.53 | 1.5 | 84±50 | 11±50 | 73±71 |
| Jun-11 | 6.2 | 0.25 | 0.5 | 21±50 | 2±25 | 19±56 |
| Dec-11 | 6.1 | 0.39 | 0.5 | -25±75 | 6±50 | -31±90 |

Notes: $S_T$ = Total settlement (Table 6); $S_{V1D}$ = Average vertical settlement due to volumetric compression using Boulanger and Idriss (2014) (BI-2014) and Zhang et al. (2002) (ZRB-2002) procedures and de Greef and Lengkeek (2018) thin-layer correction; $S_{E,L}$ = Ejecta-induced settlement as the difference between the LiDAR-based $S_T$ and $S_{V1D}$.

**Table 8b: Ejecta-Induced settlement for the top 20 m of the soil profile for the 20-m buffer for the 50th %ile PGA, $P_L$=50%, and $C_{FC}$=0.13 using BI-2014, ZRB-2002, and $I_C$ cutoff of 2.6.**

| Earthquake Event(s) | $M_W$ | PGA (g) | Depth to Groundwater (m) | $S_T$ (mm) | $S_{V1D}$ (mm) | $S_{E,L}$ (mm) |
|---|---|---|---|---|---|---|
| Sep-10 | 7.1 | 0.18 | 1.5 | 23±125 | 1±20 | 22±127 |
| Feb-11 | 6.2 | 0.53 | 1.5 | 81±50 | 11±50 | 70±71 |
| Jun-11 | 6.2 | 0.25 | 0.5 | 12±50 | 2±25 | 10±56 |
| Dec-11 | 6.1 | 0.39 | 0.5 | -21±75 | 6±50 | -27±90 |

Notes: $S_T$ = Total settlement (Table 6); $S_{V1D}$ = Average vertical settlement due to volumetric compression using Boulanger and Idriss (2014) (BI-2014) and Zhang et al. (2002) (ZRB-2002) procedures and de Greef and Lengkeek (2018) thin-layer correction; $S_{E,L}$ = Ejecta-induced settlement as the difference between the LiDAR-based $S_T$ and $S_{V1D}$.

**Table 8c: Ejecta-Induced settlement for the top 20 m of the soil profile for the 50-m buffer for the 50th %ile PGA, $P_L$=50%, and $C_{FC}$=0.13 using BI-2014, ZRB-2002, and $I_C$ cutoff of 2.6.**

| Earthquake Event(s) | $M_W$ | PGA (g) | Depth to Groundwater (m) | $S_T$ (mm) | $S_{V1D}$ (mm) | $S_{E,L}$ (mm) |
|---|---|---|---|---|---|---|
| Sep-10 | 7.1 | 0.18 | 1.5 | 32±125 | 1±20 | 31±127 |
| Feb-11 | 6.2 | 0.53 | 1.5 | 81±50 | 16±50 | 65±71 |
| Jun-11 | 6.2 | 0.25 | 0.5 | 8±50 | 2±25 | 6±56 |
| Dec-11 | 6.1 | 0.39 | 0.5 | -21±75 | 8±50 | -29±90 |

Notes: $S_T$ = Total settlement (Table 6); $S_{V1D}$ = Average vertical settlement due to volumetric compression using Boulanger and Idriss (2014) (BI-2014) and Zhang et al. (2002) (ZRB-2002) procedures and de Greef and Lengkeek (2018) thin-layer correction; $S_{E,L}$ = Ejecta-induced settlement as the difference between the LiDAR-based $S_T$ and $S_{V1D}$.

**Note 3:** The uncertainty for volumetric settlement was derived based on the sensitivity of volumetric settlement to PGA, $C_{FC}$, and $P_L$ for each earthquake event for VsVp 57203 *Shirley Intermediate School* and CC LIQ 1 – CPT 5586 – *Vivian St* sites. Taking the 50$^{th}$ percentile as the baseline case, the minimum and maximum values corresponding to the difference between the 25$^{th}$ percentile and the 50$^{th}$ percentile and the 75$^{th}$ percentile and the 50$^{th}$ percentile were determined. The arithmetic mean of the range of the minimum and maximum difference was evaluated for each patch at the two sites. The maximum arithmetic mean for each earthquake event was rounded to the nearest five and used as the uncertainty value. Accordingly, the 1-D volumetric settlement uncertainties of ±20, ±50, ±25, and ±50 mm for the Sep-10, Feb-11, Jun-11, and Dec-11 earthquake events, respectively, were used for all sites in this study.

**Table 9a: Coverage area and height of ejecta estimates for the 10-m buffer using photographs.**

| Earthquake Event | $A_{E,thick}$ ($m^2$) | $H_{E,thick}$ (mm) | $A_{E,thin}$ ($m^2$) | $H_{E,thin}$ (mm) | $A_T$ ($m^2$) |
|---|---|---|---|---|---|
| Sep-10 | 0 | 0 | 0 | 0 | 155 |
| Feb-11 | 0 | 0 | 0 | 0 | 155 |
| Jun-11 | 0 | 0 | 0 | 0 | 155 |
| Dec-11 | 0 | 0 | 0 | 0 | 155 |

Notes: $A_{E,thick/thin}$ = Coverage area of thick/thin ejecta layers; $H_{E,thick/thin}$ = Lower-upper estimate of height of thick/thin ejecta layers; $A_T$ = Total assessment area of a buffer being considered; Thin and thick layers correspond to light gray and dark gray colors of ejecta observed in aerial photography.

**Table 9b: Coverage area and height of ejecta estimates for the 20-m buffer using photographs.**

| Earthquake Event | $A_{E,thick}$ ($m^2$) | $H_{E,thick}$ (mm) | $A_{E,thin}$ ($m^2$) | $H_{E,thin}$ (mm) | $A_T$ ($m^2$) |
|---|---|---|---|---|---|
| Sep-10 | 0 | 0 | 0 | 0 | 514 |
| Feb-11 | 0 | 0 | 0 | 0 | 514 |
| Jun-11 | 0 | 0 | 0 | 0 | 514 |
| Dec-11 | 0 | 0 | 0 | 0 | 514 |

Notes: $A_{E,thick/thin}$ = Coverage area of thick/thin ejecta layers; $H_{E,thick/thin}$ = Lower-upper estimate of height of thick/thin ejecta layers; $A_T$ = Total assessment area of a buffer being considered; Thin and thick layers correspond to light gray and dark gray colors of ejecta observed in aerial photography.

**Table 9c: Coverage area and height of ejecta estimates for the 50-m buffer using photographs.**

| Earthquake Event | $A_{E,thick}$ ($m^2$) | $H_{E,thick}$ (m) | $A_{E,thin}$ ($m^2$) | $H_{E,thin}$ (m) | $A_T$ ($m^2$) |
|---|---|---|---|---|---|
| Sep-10 | 0 | 0 | 0 | 0 | 1479 |
| Feb-11 | 0 | 0 | 0 | 0 | 1479 |
| Jun-11 | 0 | 0 | 0 | 0 | 1479 |
| Dec-11 | 0 | 0 | 0 | 0 | 1479 |

Notes: $A_{E,thick/thin}$ =Coverage area of thick/thin ejecta layers; $H_{E,thick/thin}$ = Lower-upper estimate of height of thick/thin ejecta layers; $A_T$= Total assessment area of a buffer being considered; Thin and thick layers correspond to light gray and dark gray colors of ejecta observed in aerial photography.

**Note 4:** The values in Table 9 are based on the high-resolution aerial photographs of the site (Figures 64 through 67). The ejecta is not visible at the site within the assessment area for any earthquake event.

**Table 10: Ejecta-induced settlement estimates based on photography.**

| Earthquake Event | 10-m buffer | | 20-m buffer | | 50-m buffer | |
|---|---|---|---|---|---|---|
| | $S_{E,P,lower}$ (mm) | $S_{E,P,upper}$ (mm) | $S_{E,P,lower}$ (mm) | $S_{E,P,upper}$ (mm) | $S_{E,P,lower}$ (mm) | $S_{E,P,upper}$ (mm) |
| Sep-10 | 0 | 0 | 0 | 0 | 0 | 0 |
| Feb-11 | 0 | 0 | 0 | 0 | 0 | 0 |
| Jun-11 | 0 | 0 | 0 | 0 | 0 | 0 |
| Dec-11 | 0 | 0 | 0 | 0 | 0 | 0 |

Note: $S_{E,P,lower}$ and $S_{E,P,upper}$ correspond to lower and upper estimates of $S_{E,P}$, respectively.

**Table 11: Best final estimates of ejecta-induced settlement.**

| EQ Event | 10-m buffer | | | 20-m buffer | | | 50-m buffer | | |
|---|---|---|---|---|---|---|---|---|---|
| | $S_{E,L}$ (mm) | $S_{E,P}$ (mm) | $S_{E,final}$ (mm) | $S_{E,L}$ (mm) | $S_{E,P}$ (mm) | $S_{E,final}$ (mm) | $S_{E,L}$ (mm) | $S_{E,P}$ (mm) | $S_{E,final}$ (mm) |
| Sep-10 | 32±127 | 0 | 0 | 22±127 | 0 | 0 | 31±127 | 0 | 0 |
| Feb-11 | 73±71 | 0 | 0 | 70±71 | 0 | 0 | 65±71 | 0 | 0 |
| Jun-11 | 19±56 | 0 | 0 | 10±56 | 0 | 0 | 6±56 | 0 | 0 |
| Dec-11 | -31±90 | 0 | 0 | -27±90 | 0 | 0 | -29±90 | 0 | 0 |

Notes: $S_{E,L}$ = Ejecta-induced settlement based on LiDAR data reported in Table 8; $S_{E,P}$ = Median ejecta-induced settlement for the range of values reported in Table 10; $S_{E,final}$ = Best final estimate of ejecta-induced settlement rounded to the nearest 5; Final plus/minus values are also rounded to the nearest 5.

**Note 5:**

- $S_{E,final}$ is based solely on $S_{E,P}$ due to the availability of the high-resolution aerial photographs for all earthquake events that show no liquefaction ejecta at the site within the assessment area (Patch A). The aerial photograph for the Dec-11 earthquake shows negligible ejecta (<5 mm) on the road, within the 50-m buffer. As a side note, the site is not in the apparent zone of higher/lower ground surface subsidence compared to the adjacent areas for any earthquake event and the LiDAR surveys are not affected by ejecta. The Rawhiti Domain site is in the zone of accurate LPI prediction of liquefaction severity for the Sep-11 and Feb-11 earthquakes (Maurer et al. 2014[3]).
- There were minor ejecta on the road (<5 mm) for the Dec-11 EQ.

<u>Summary</u>:

**The best estimate of the ejecta-induced free-field ground settlement at the Rawhiti Domain site for the SEP 2010, FEB 2011, JUN 2011, and DEC 2011 earthquake is 0 mm, 0 mm, 0 mm, and 0 mm, respectively.**

[3] Maurer, B. W., Green, R. A., Cubrinovski, M., & Bradley, B. A. (2014). Evaluation of the Liquefaction Potential Index for Assessing Liquefaction Hazard in Christchurch, New Zealand. *Journal of Geotechnical and Geoenvironmental Engineering*, 140(7), 04014032-1-11. doi:10.1061/(asce)gt.1943-5606.0001117


**Figure 5: Location of the site.**


**Figure 6: Position of the site relative to nearby buildings, vegetation, and free-face features.**


Figure 7: Street view of the flat land.


Figure 8: Satellite image of the site taken in Dec 2004.

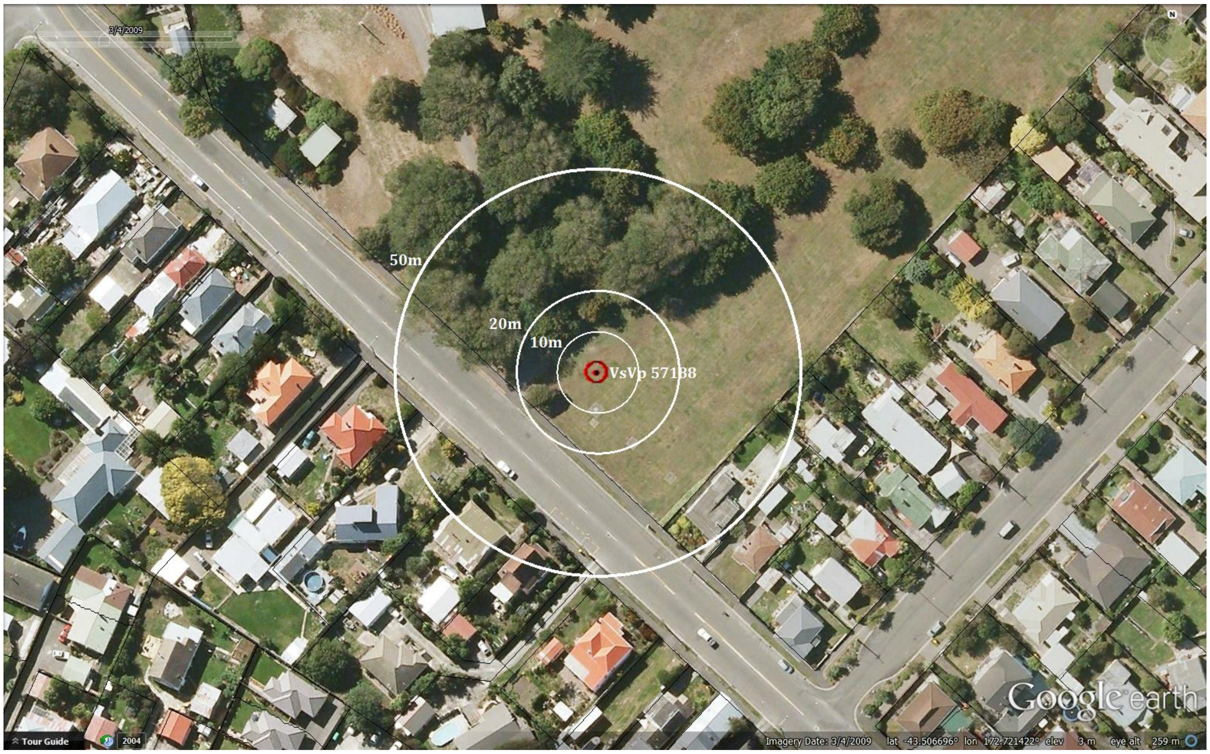


Figure 9: Satellite image of the site taken in March 2009.

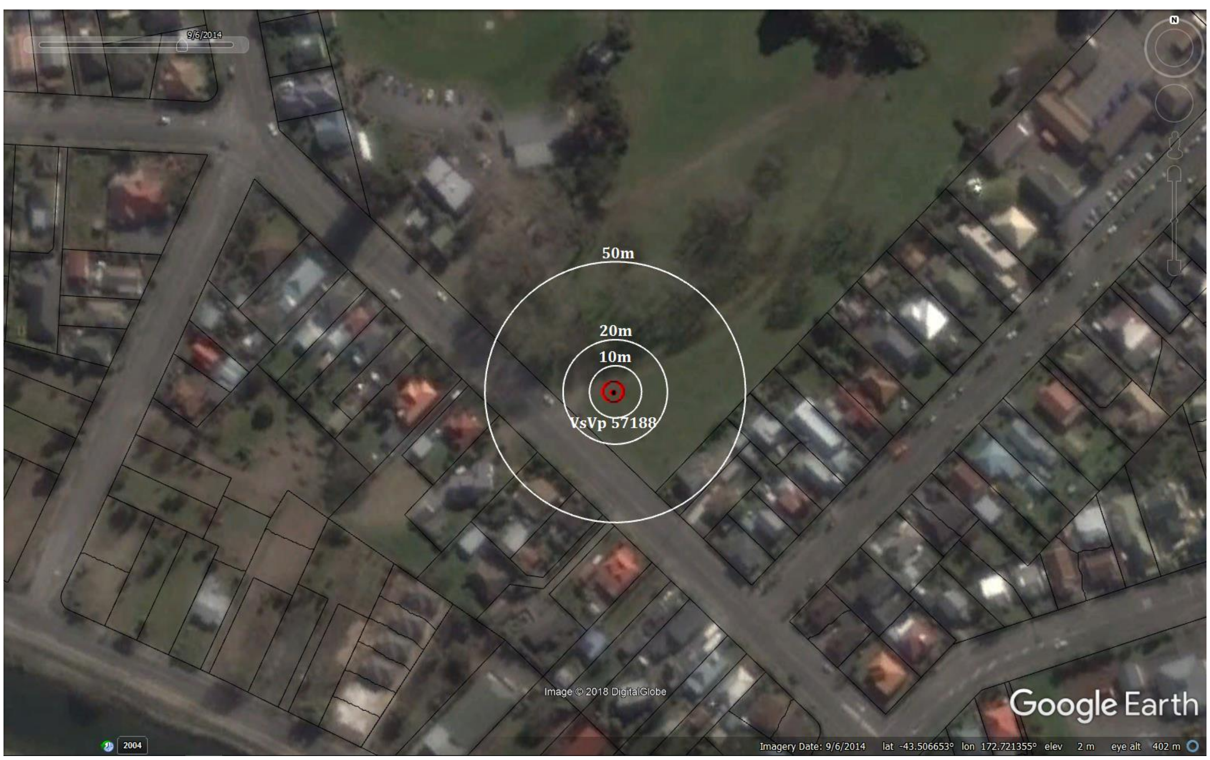


Figure 10: Satellite image of the site taken in Sep 2014.


**Figure 11: Satellite image of the site taken in Jan 2015.**


**Figure 12: Satellite image of the site taken in June 2015.**

Figure 13: EQC Aerial Photograph of the site taken on Sep 4, 2010.

Figure 14: EQC Aerial Photograph of the site taken on Sep 4, 2010; enlarged view.


Figure 15: EQC Aerial Photograph of the site taken on Feb 24, 2011.

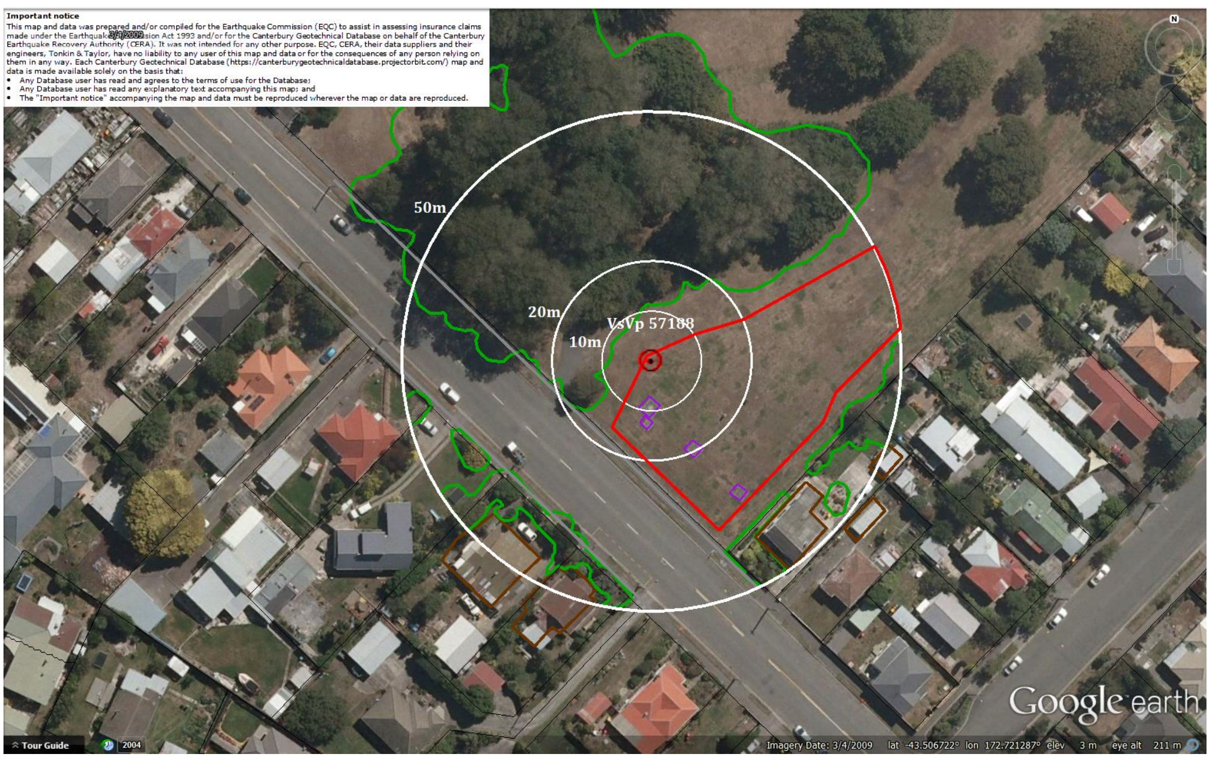


Figure 16: EQC Aerial Photograph of the site taken on Feb 24, 2011; enlarged view.


Figure 17: EQC Aerial Photograph of the site taken on June 14-15, 2011.

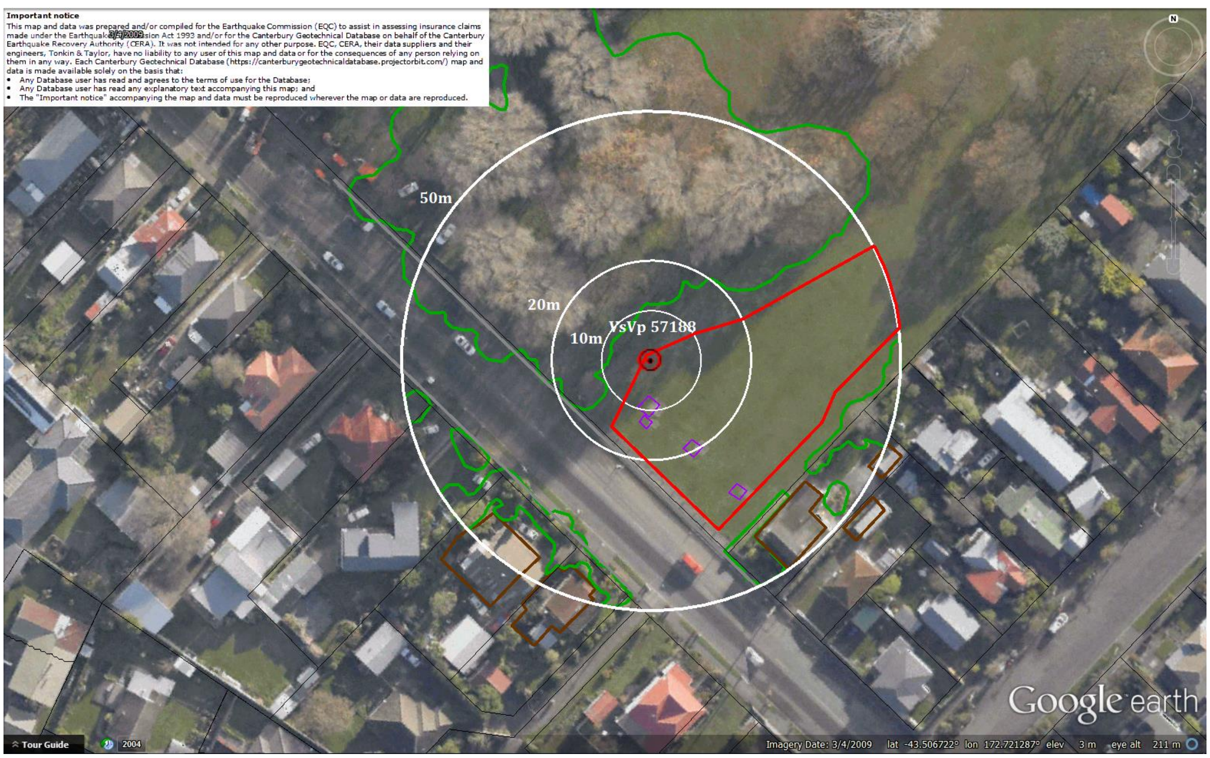


Figure 18: EQC Aerial Photograph of the site taken on June 14-15, 2011; enlarged view.


**Figure 19: EQC Aerial Photograph of the site taken on Dec 24, 2011.**

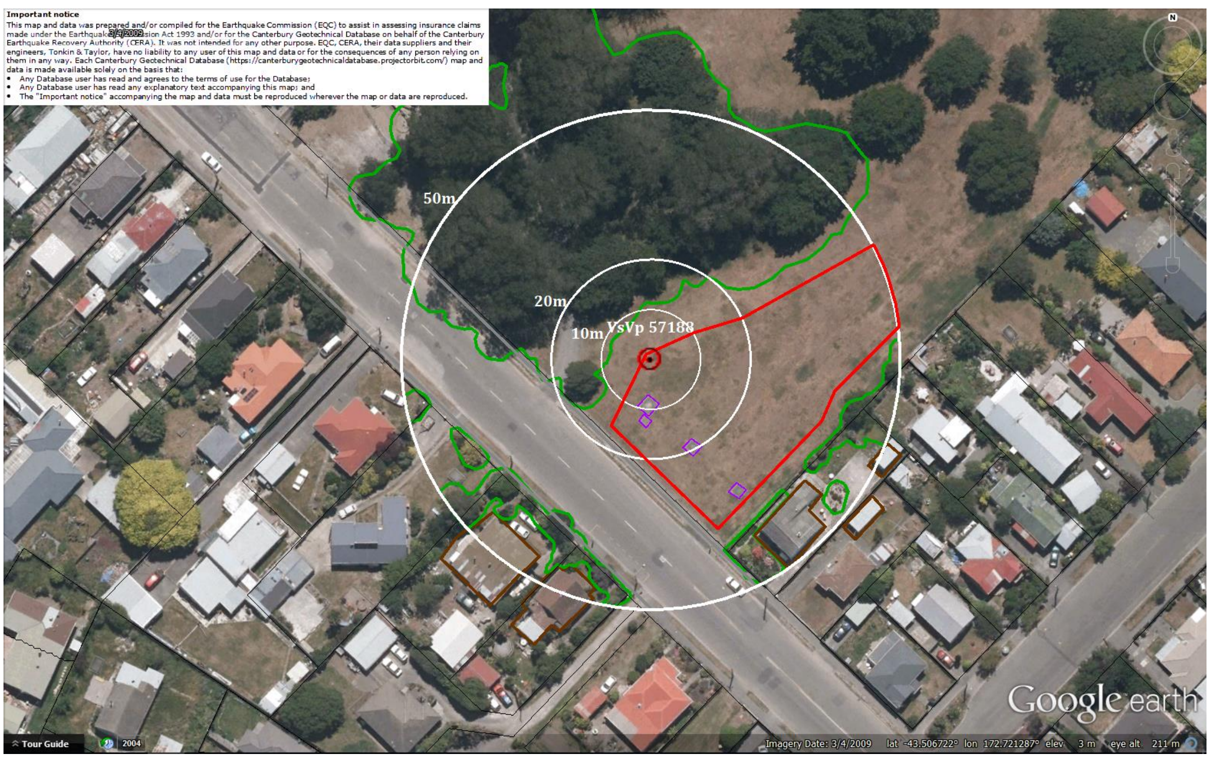


**Figure 20: EQC Aerial Photograph of the site taken on Dec 24, 2011; enlarged view.**

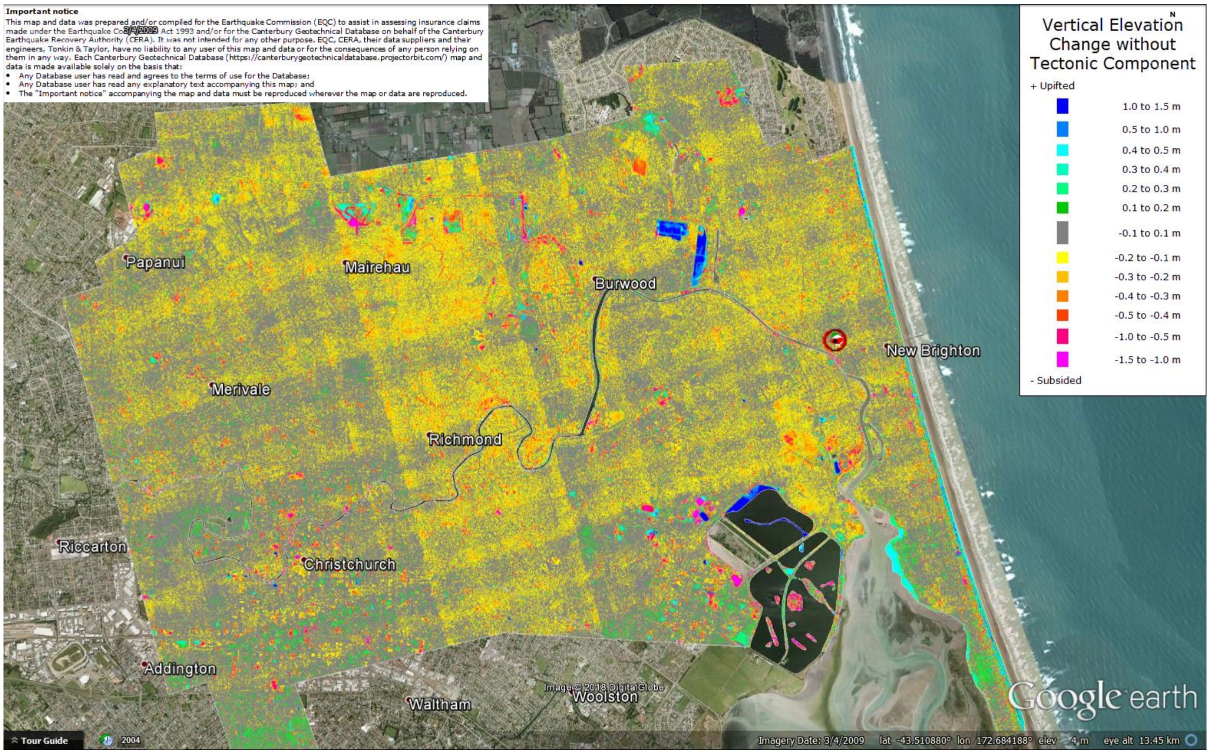


**Figure 21: Vertical Ground Movements (Surface – Tectonic) for Sep 2010 Earthquake – the site is not in the apparent zone of overestimated ground surface subsidence.**

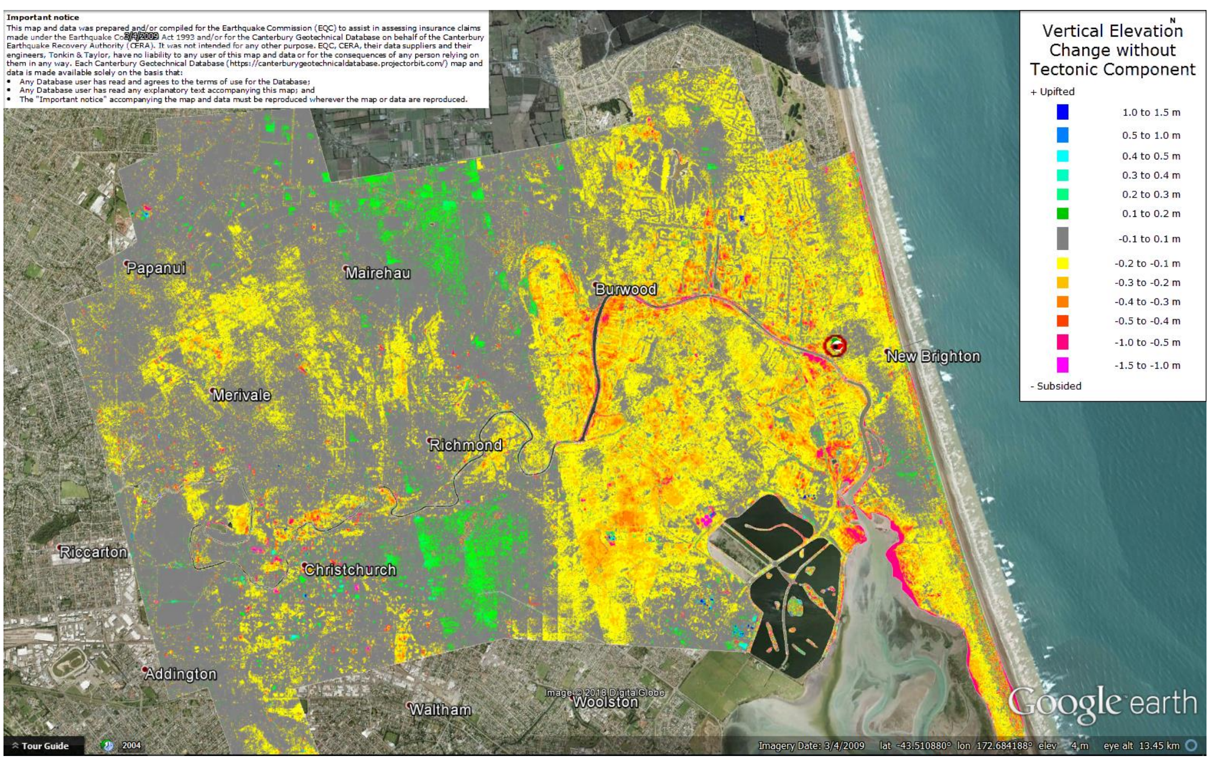


**Figure 22: Vertical Ground Movements (Surface – Tectonic) for Feb 2011 Earthquake – the site is not in the apparent zone of underestimated ground surface subsidence.**

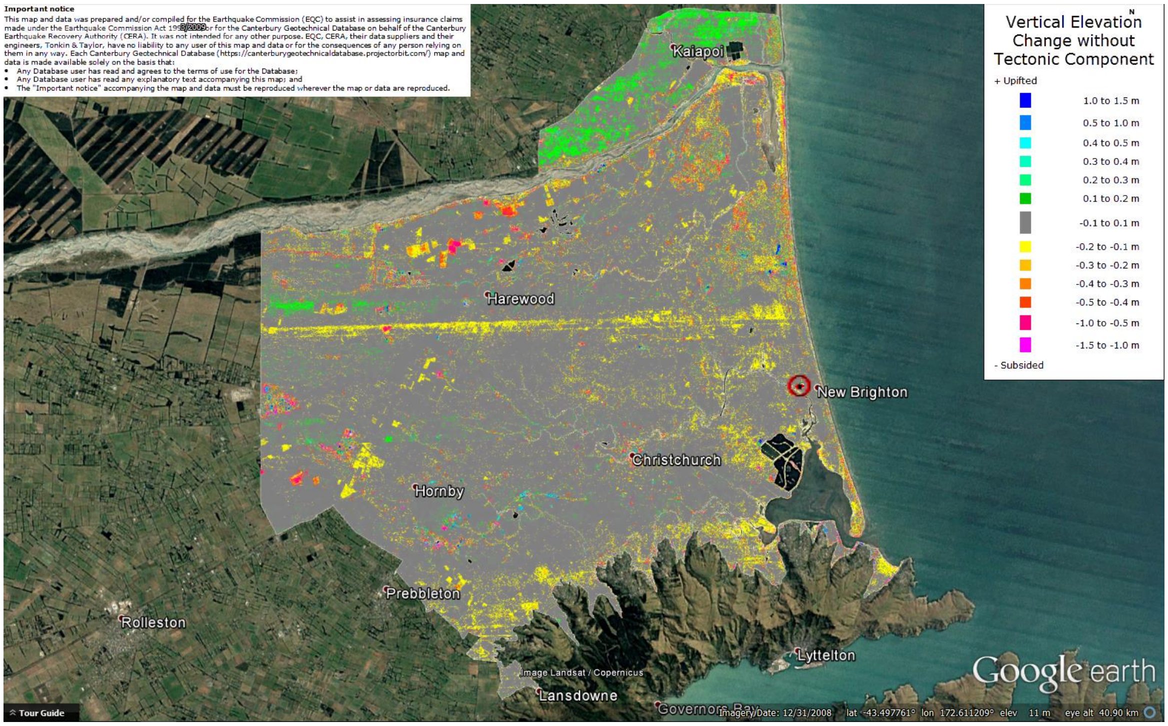


Figure 23: Vertical Ground Movements (Surface – Tectonic) for June 2011 Earthquake – the site is not in the apparent zone of overestimated or underestimated ground surface subsidence.

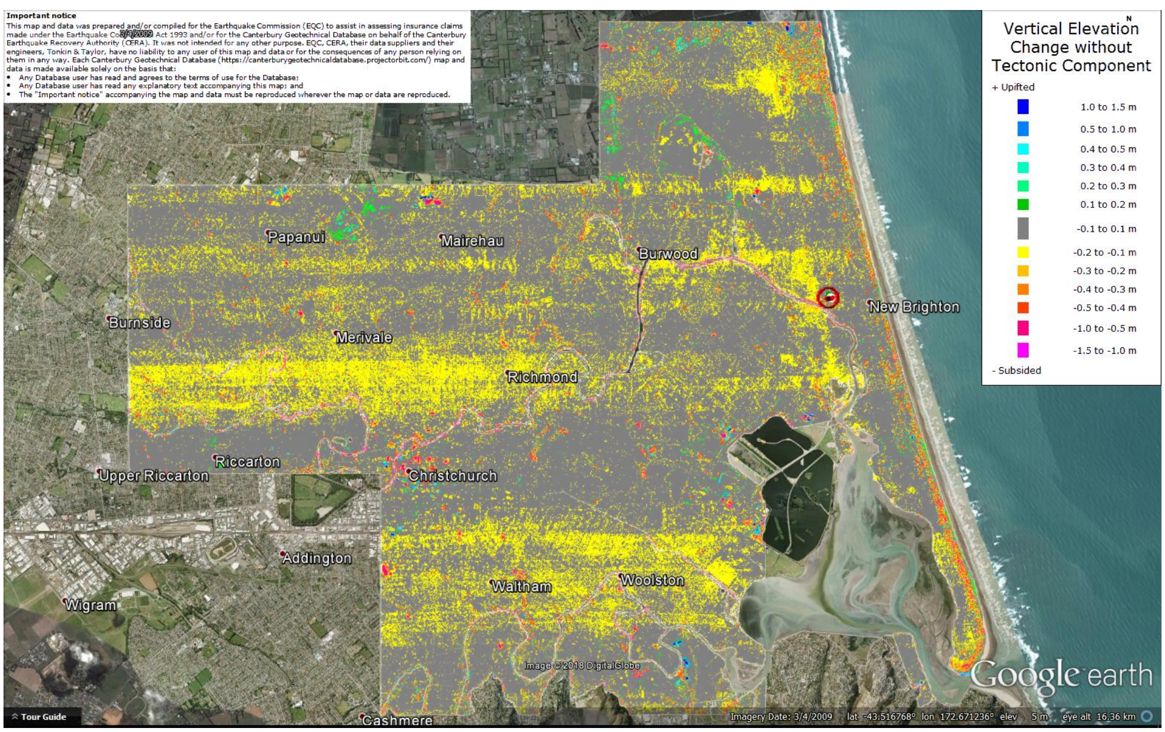


Figure 24: Vertical Ground Movements (Surface – Tectonic) for Dec 2011 Earthquake – the site is not in the apparent zone of overestimated or underestimated ground surface subsidence.

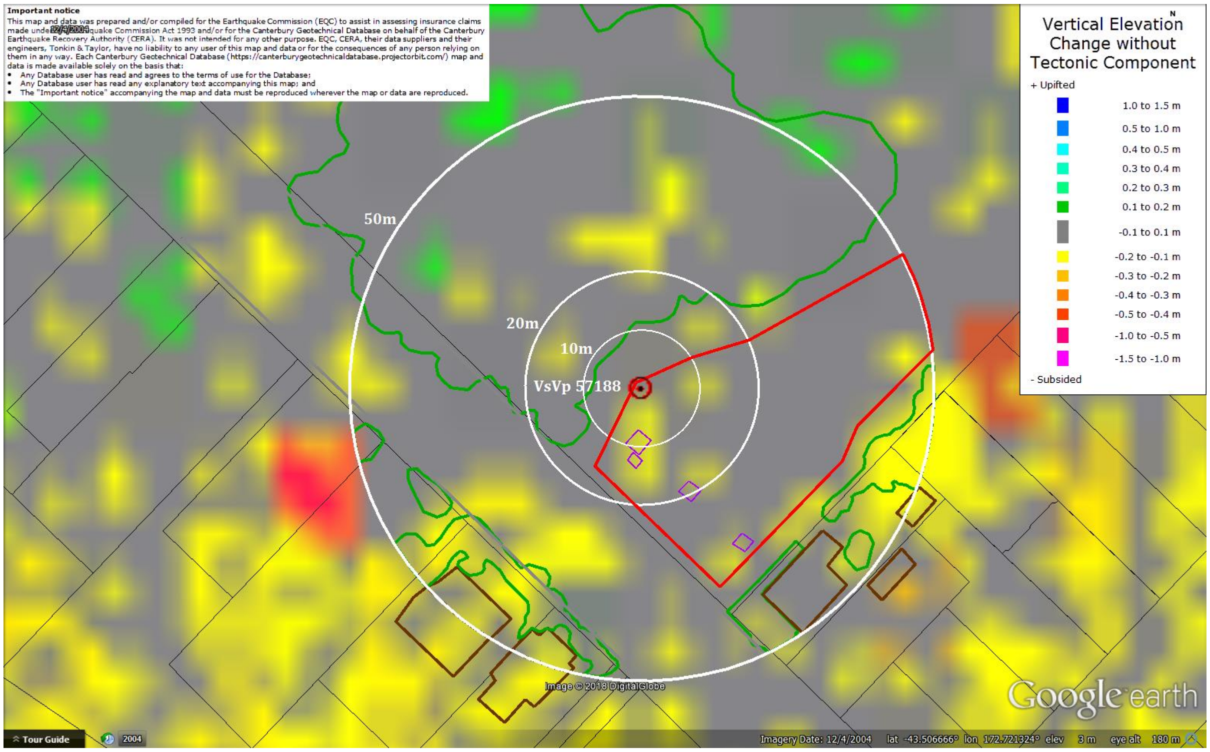


**Figure 25: Ground surface subsidence without tectonic component for Sep 2010 Earthquake according to the LiDAR DEM.**

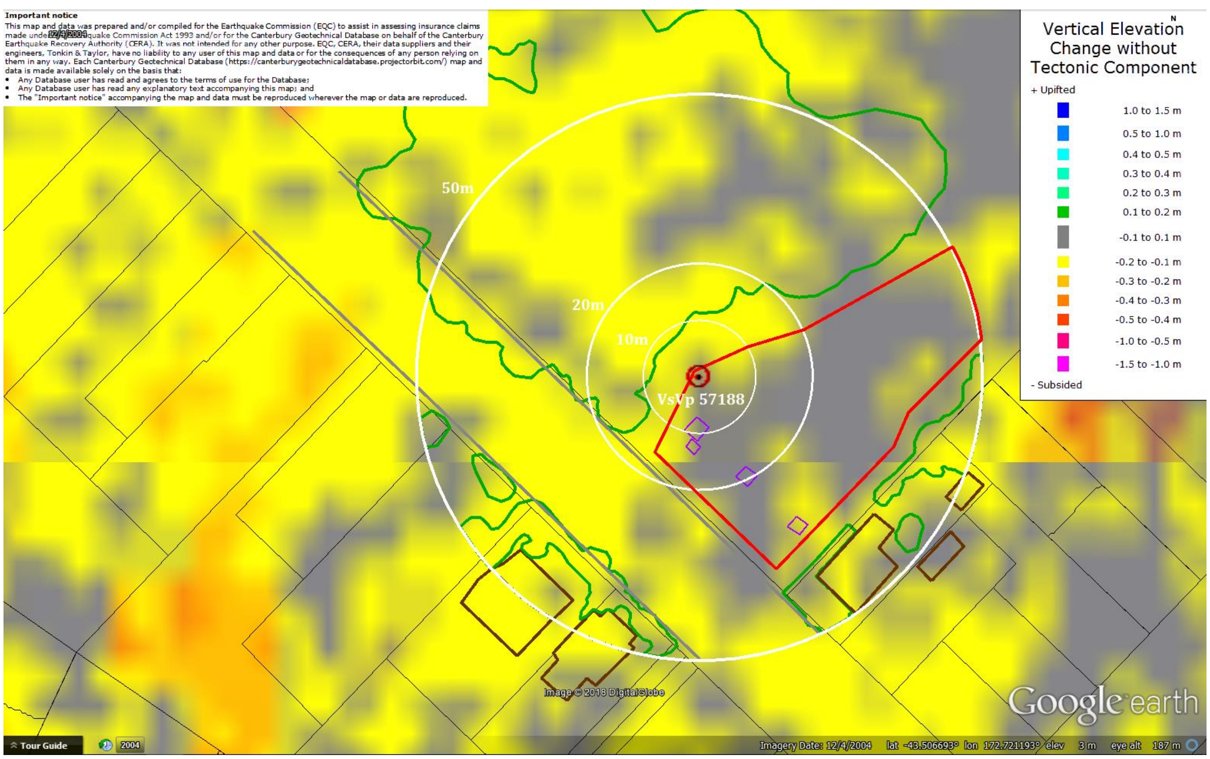


**Figure 26: Ground surface subsidence without tectonic component for Feb 2011 Earthquake according to the LiDAR DEM.**

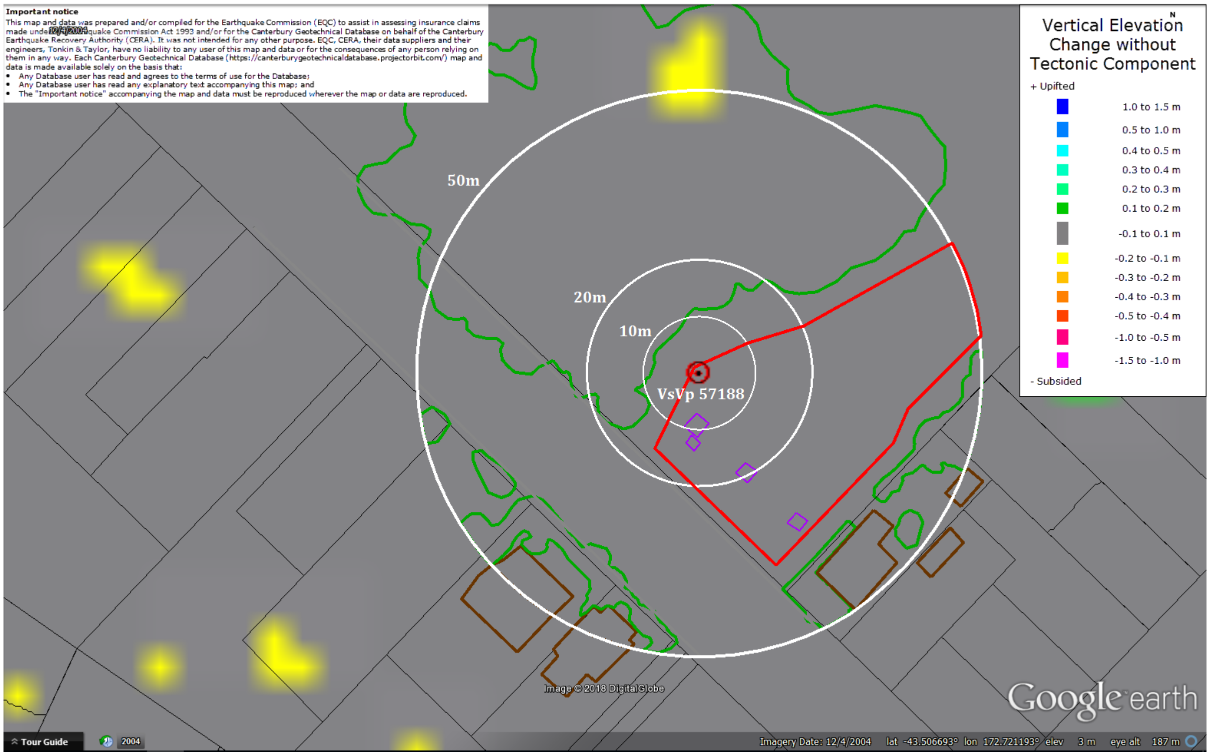


**Figure 27: Ground surface subsidence without tectonic component for Jun 2011 Earthquake according to the LiDAR DEM.**

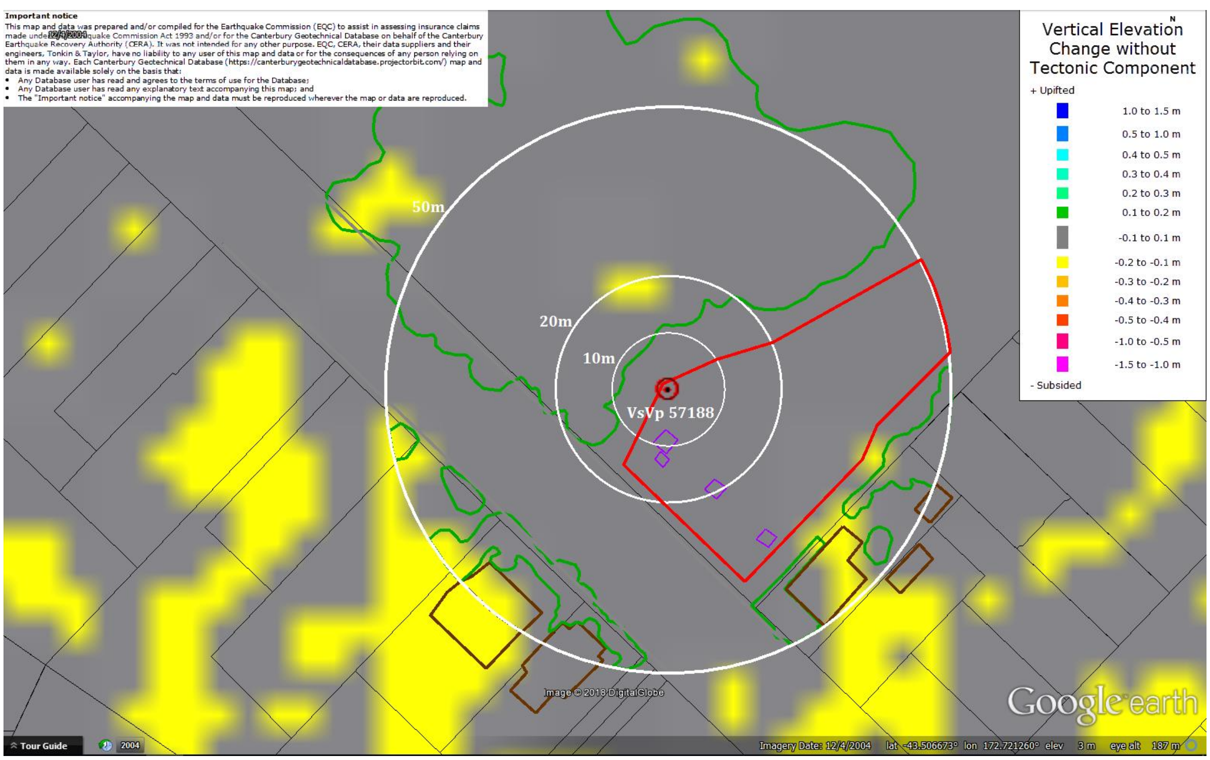


**Figure 28: Ground surface subsidence without tectonic component for Dec 2011 Earthquake according to the LiDAR DEM.**

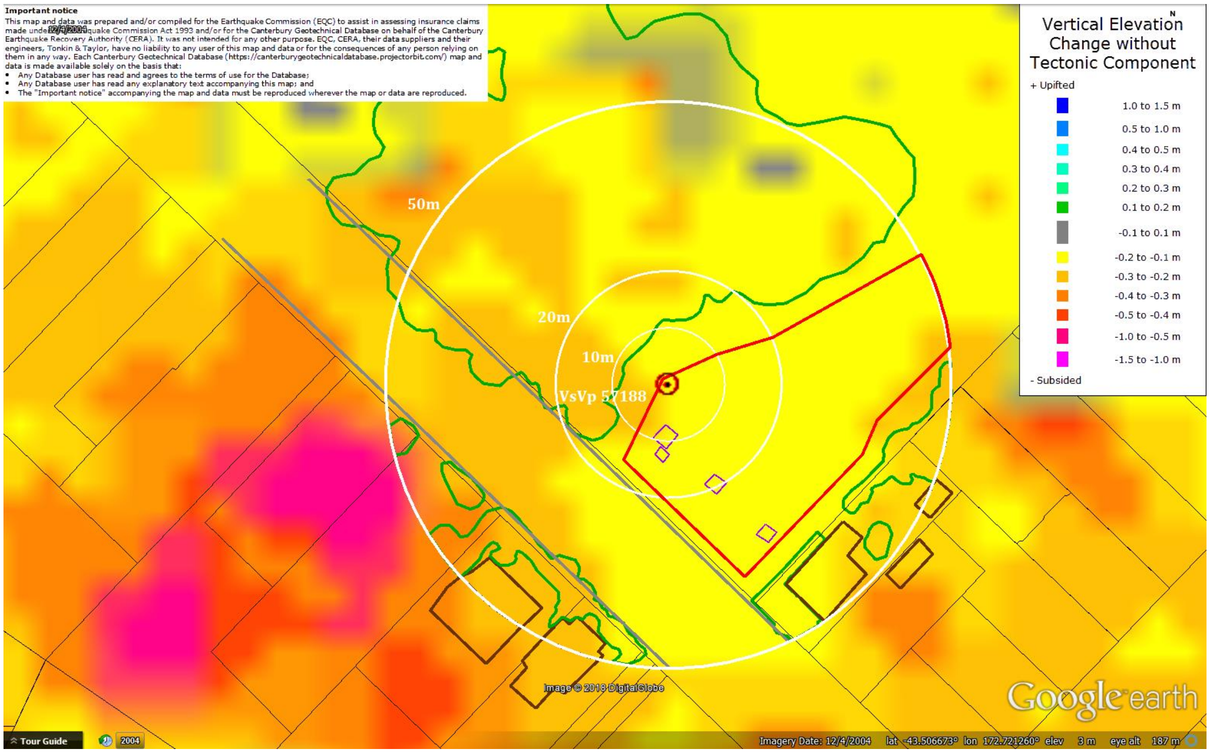


**Figure 29: Ground surface subsidence without tectonic component for Canterbury Earthquake Sequence according to the LiDAR DEM.**

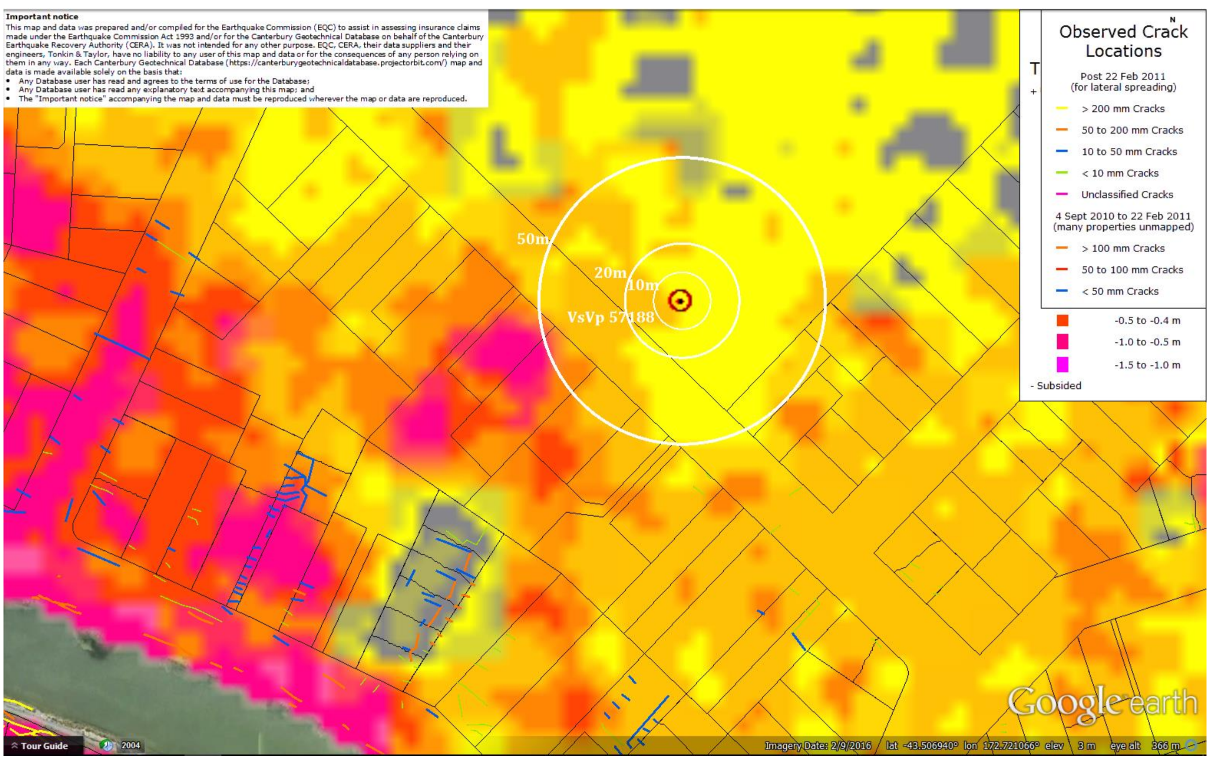


**Figure 30: Absence of ground cracks indicating no lateral spreading for Canterbury Earthquake Sequence.**

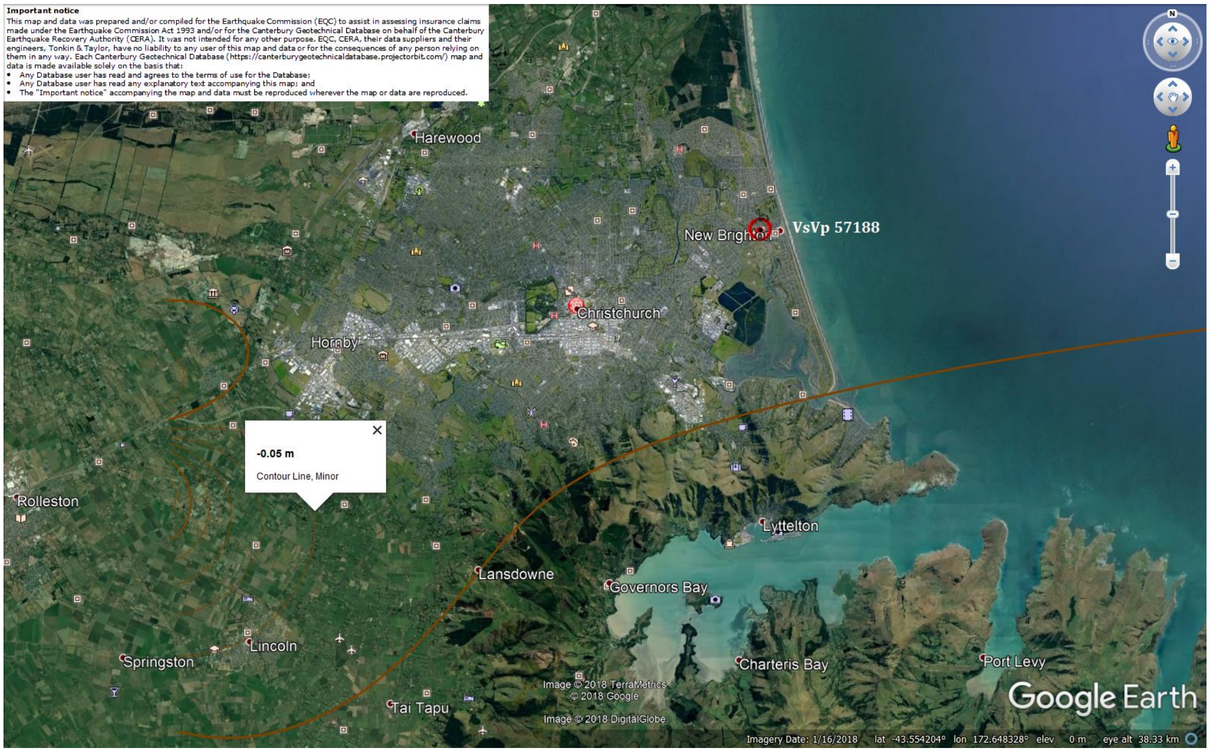


Figure 31: Vertical tectonic movements for Sep 2010 Earthquake.

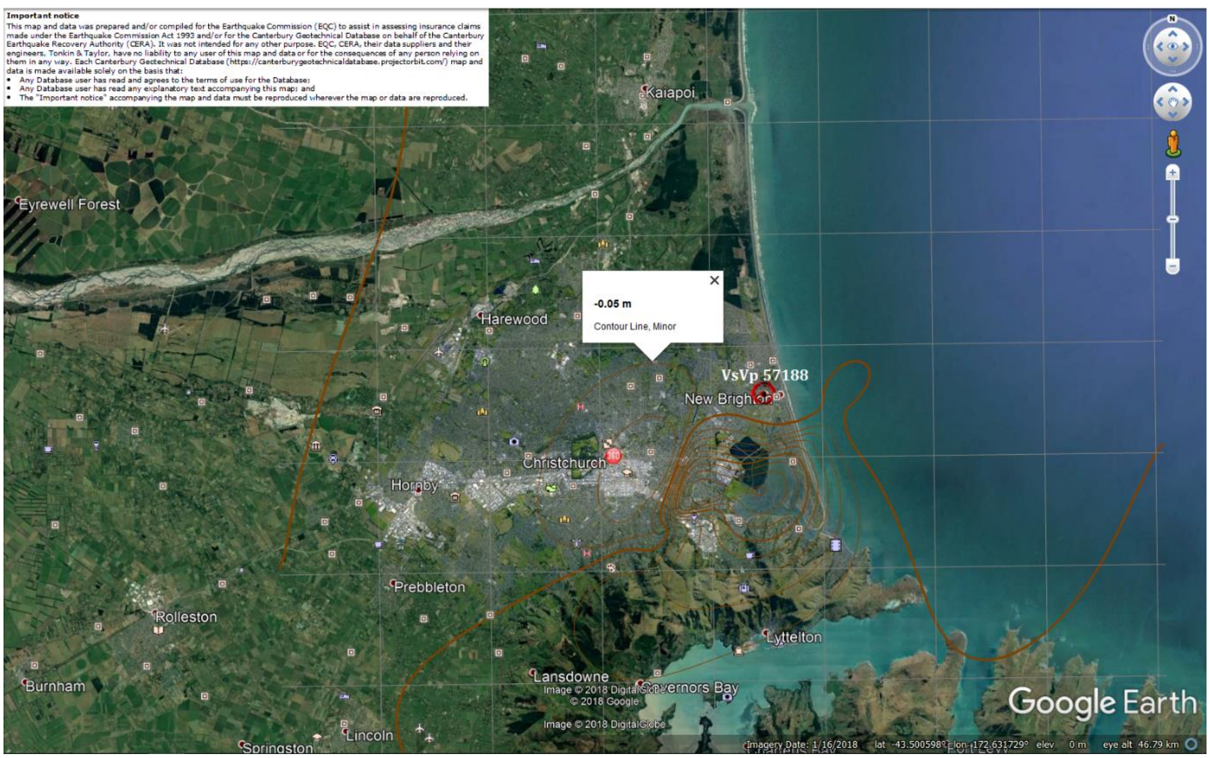


Figure 32: Vertical tectonic movements for Feb 2011 Earthquake.

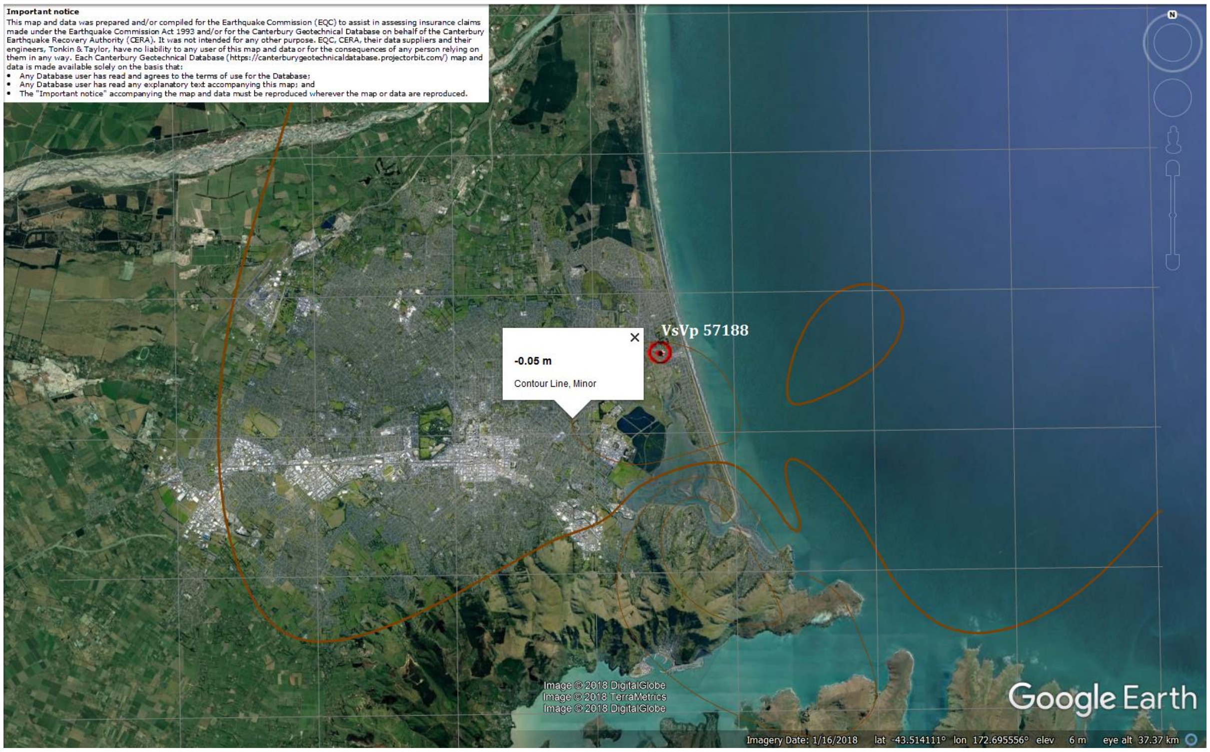


Figure 33: Vertical tectonic movements for June 2011 Earthquake.


Figure 34: Vertical tectonic movements for Dec 2011 Earthquake.

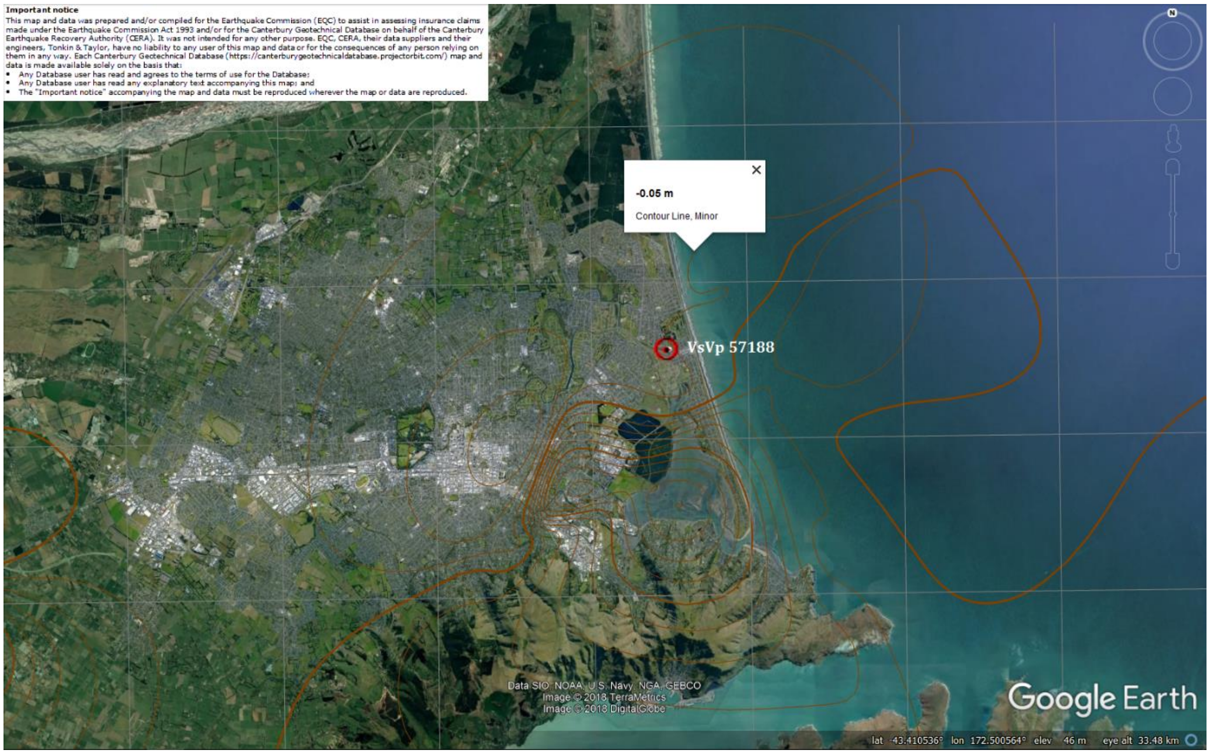


Figure 35: Vertical tectonic movements for Canterbury Earthquake Sequence.

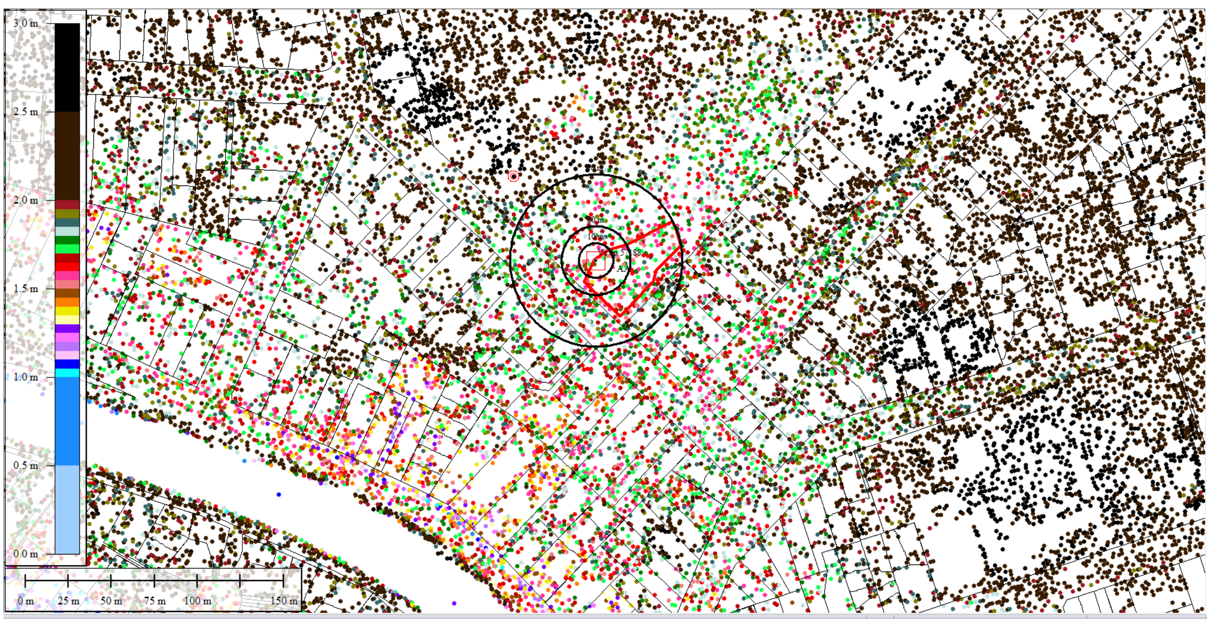


Figure 36: Jul 2003 LiDAR survey.

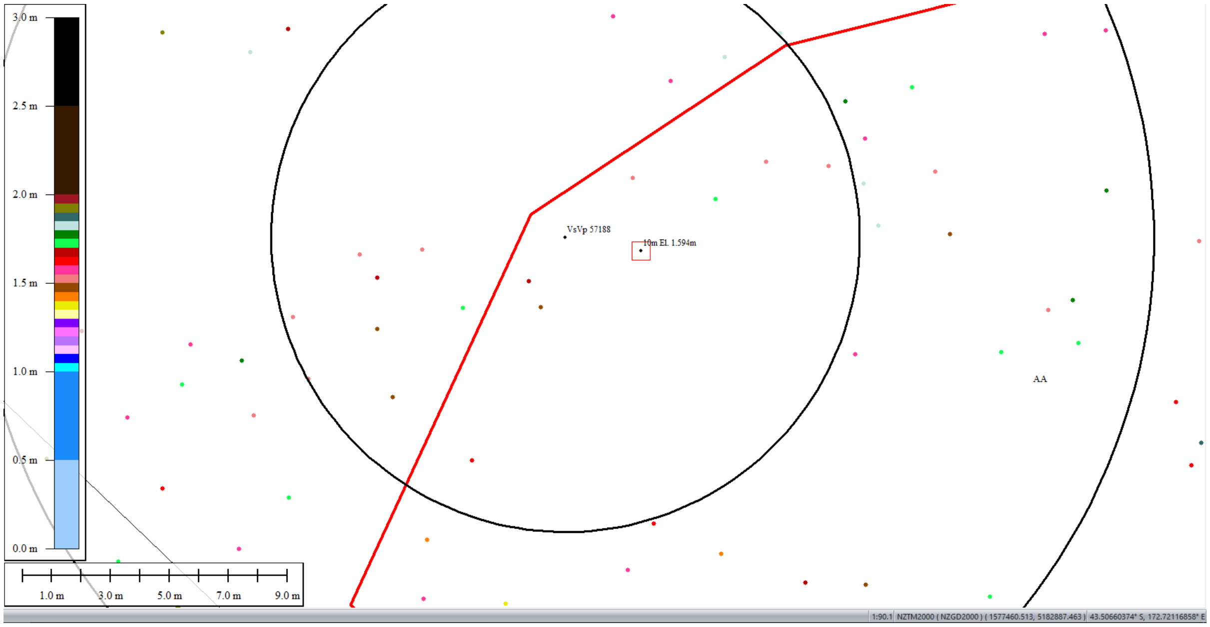


Figure 37: Ground surface elevation averaged over 10-m buffer for Jul 2003 LiDAR survey.

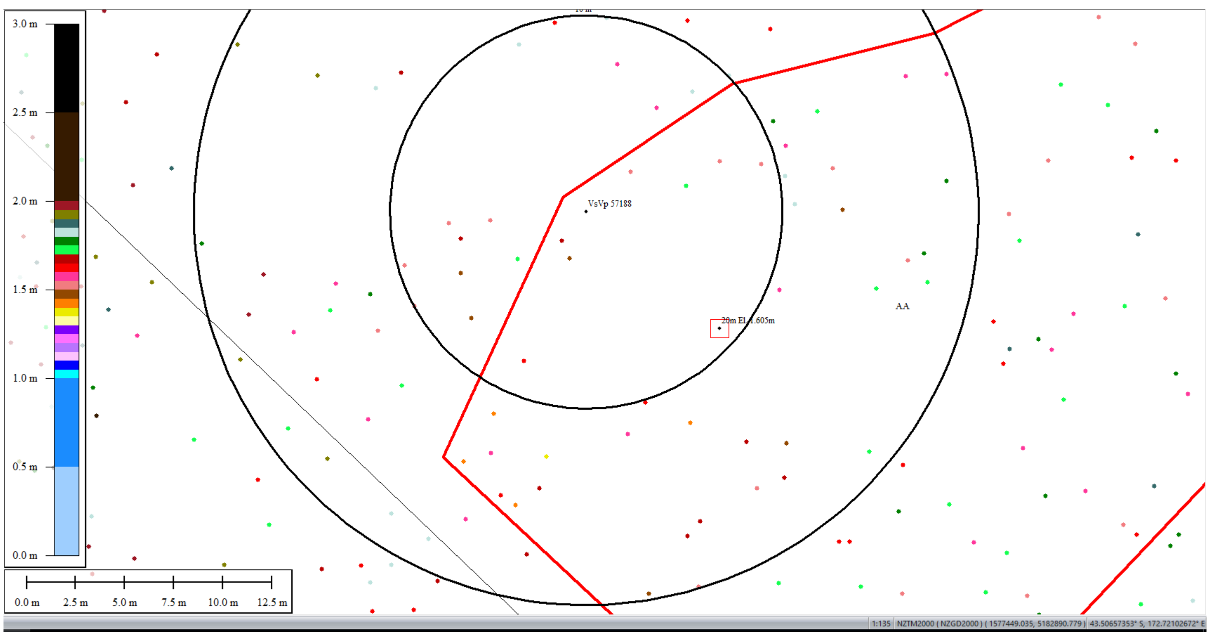


Figure 38: Ground surface elevation averaged over 20-m buffer for Jul 2003 LiDAR survey.

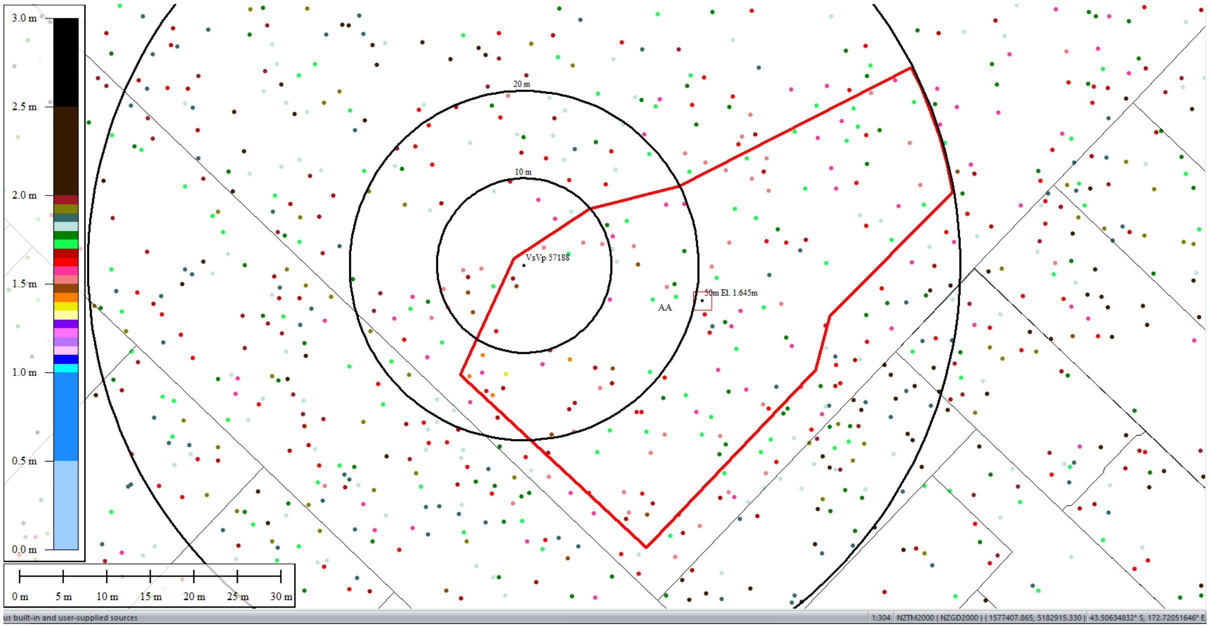


Figure 39: Ground surface elevation averaged over 50-m buffer for Jul 2003 LiDAR survey.

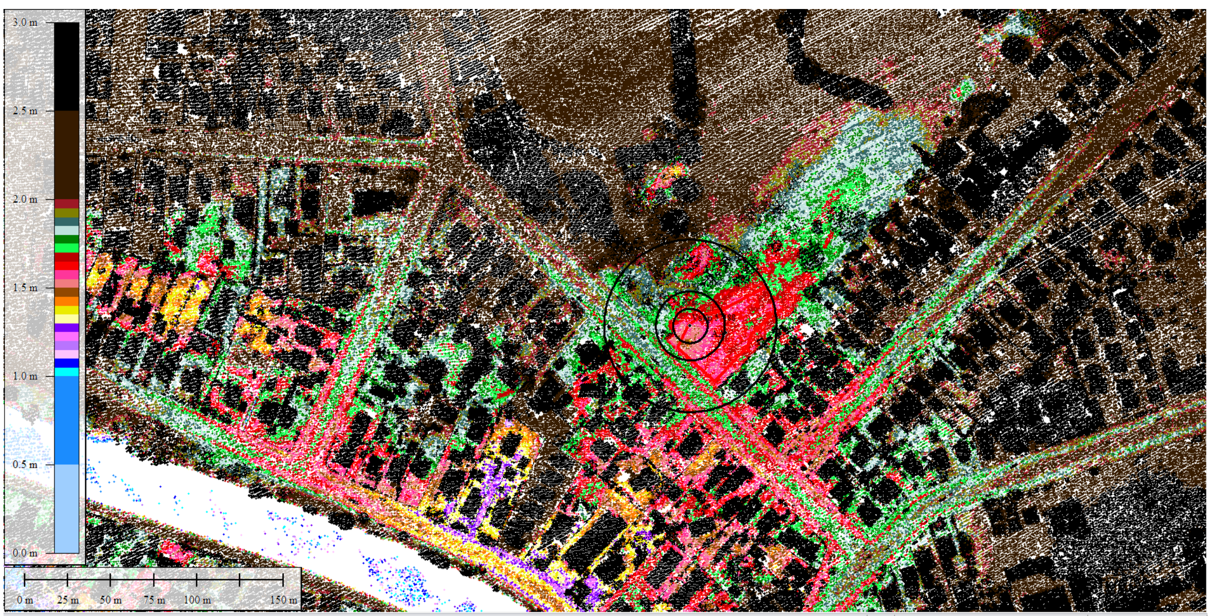


Figure 40: Sep 5, 2010 LiDAR survey.

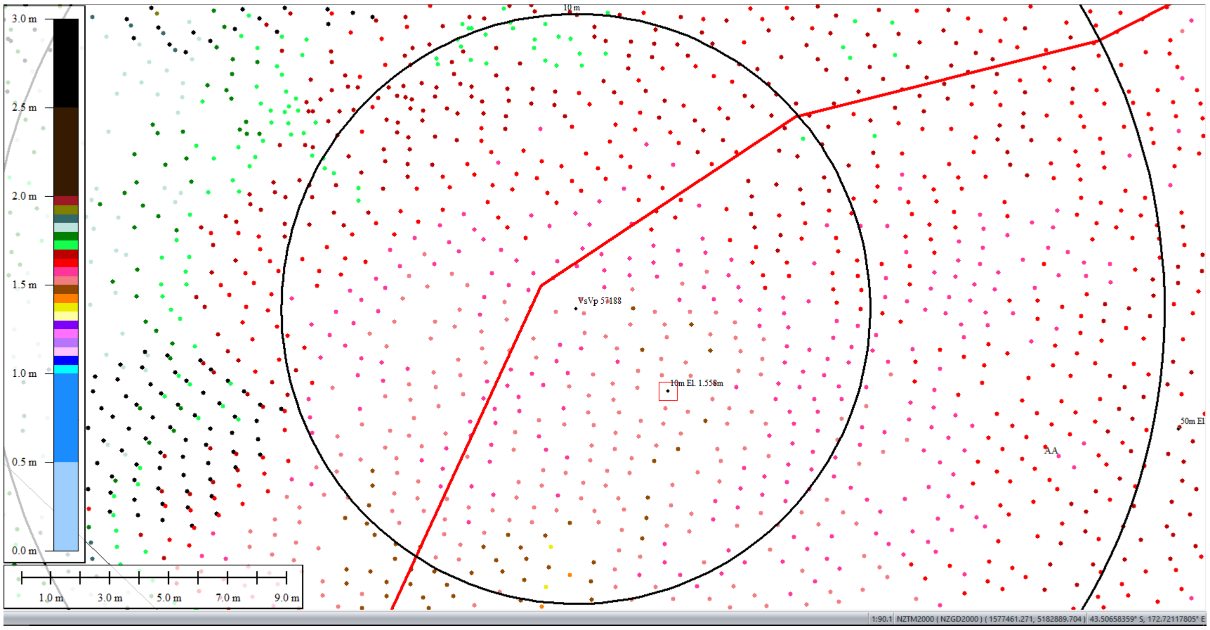


**Figure 41: Ground surface elevation averaged over 10-m buffer for Sep 5, 2010 LiDAR survey.**

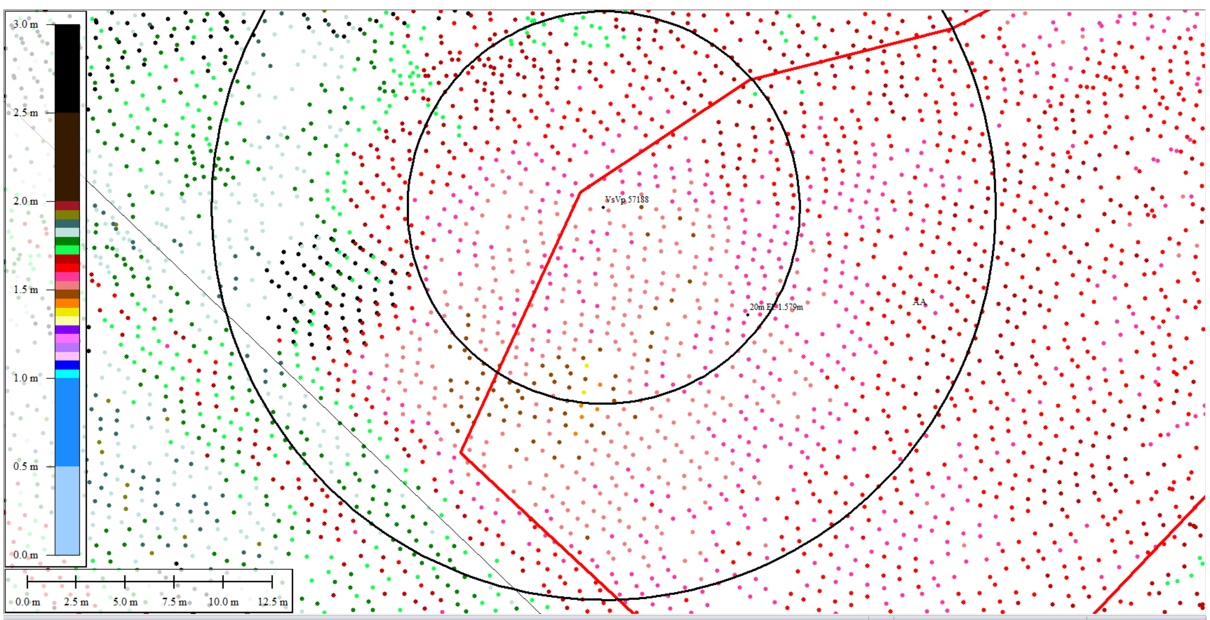


**Figure 42: Ground surface elevation averaged over 20-m buffer for Sep 5, 2010 LiDAR survey.**

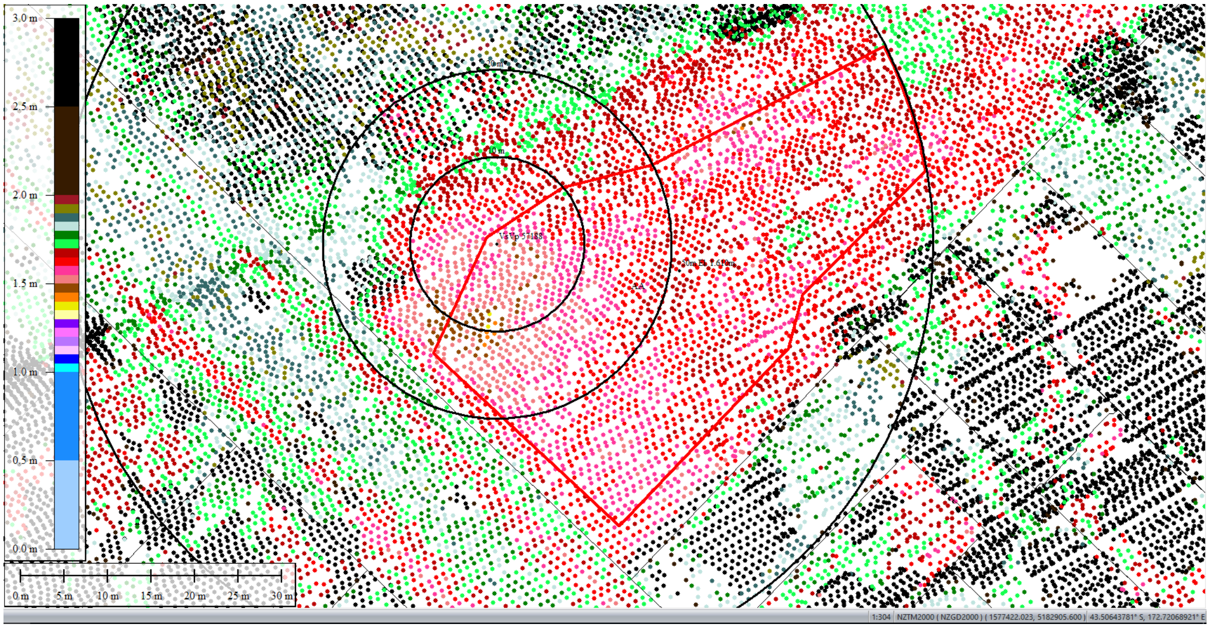


**Figure 43: Ground surface elevation averaged over 50-m buffer for Sep 5, 2010 LiDAR survey.**

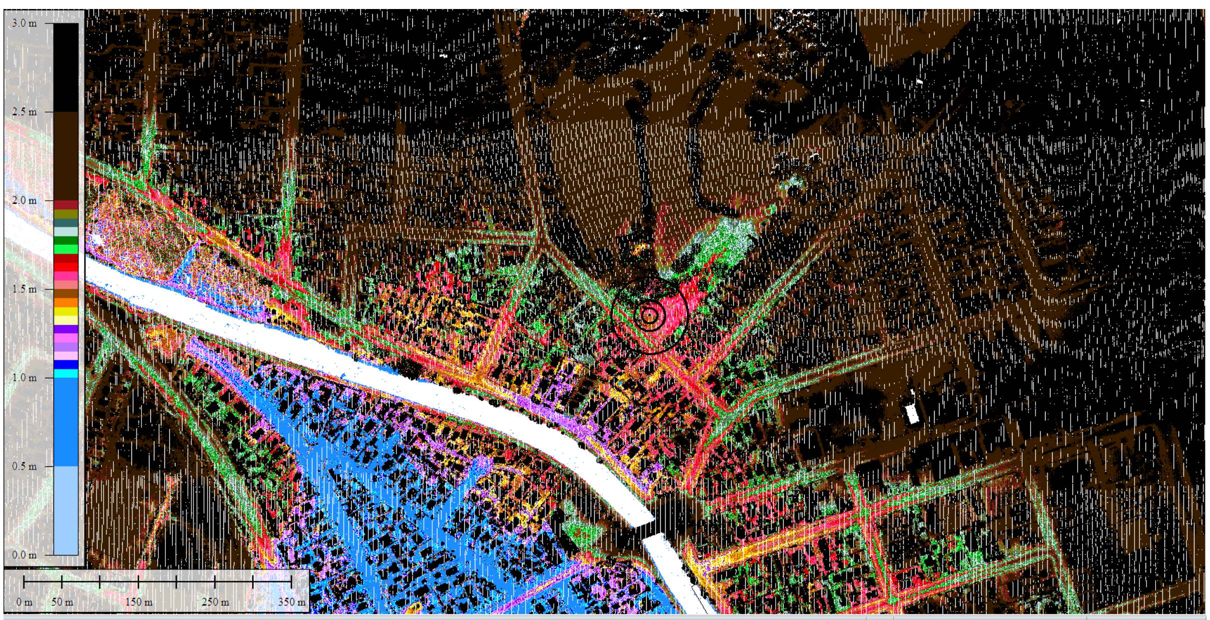


**Figure 44: Mar 2011 LiDAR survey.**

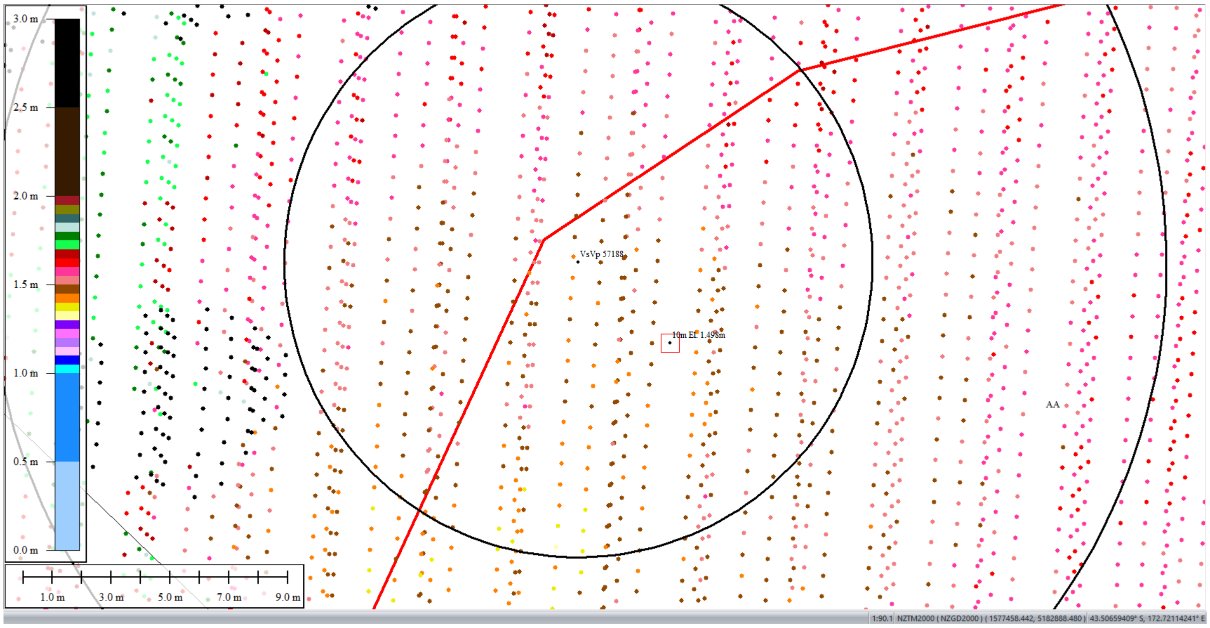


**Figure 45: Ground surface elevation averaged over 10-m buffer for Mar 2011 LiDAR survey.**

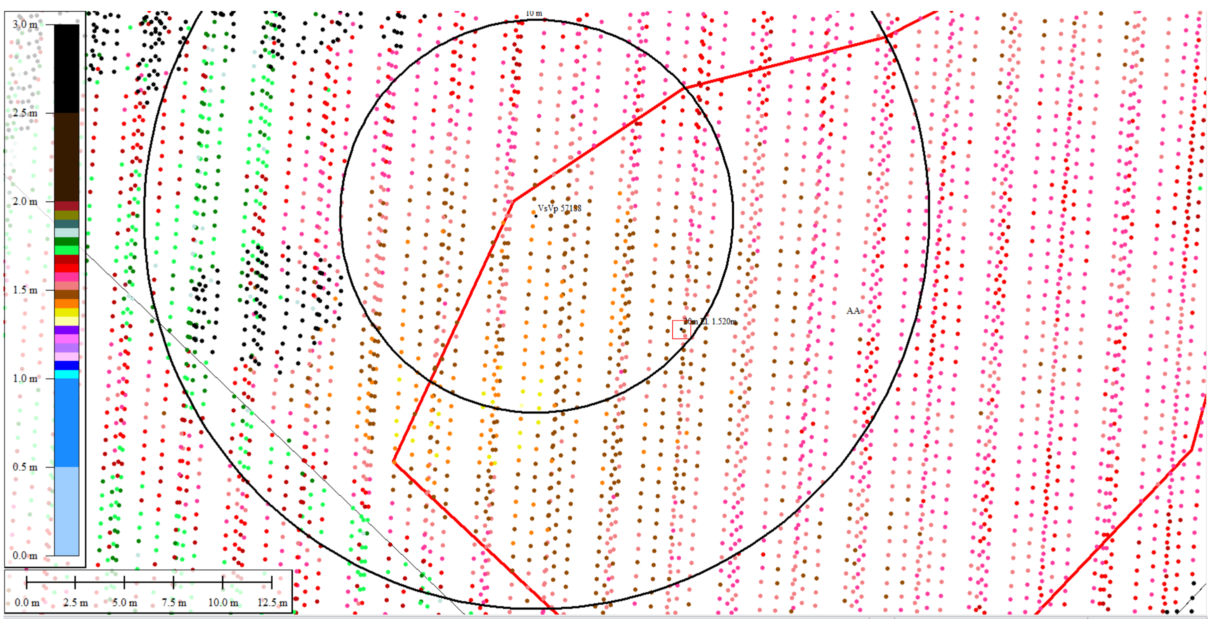


**Figure 46: Ground surface elevation averaged over 20-m buffer for Mar 2011 LiDAR survey.**

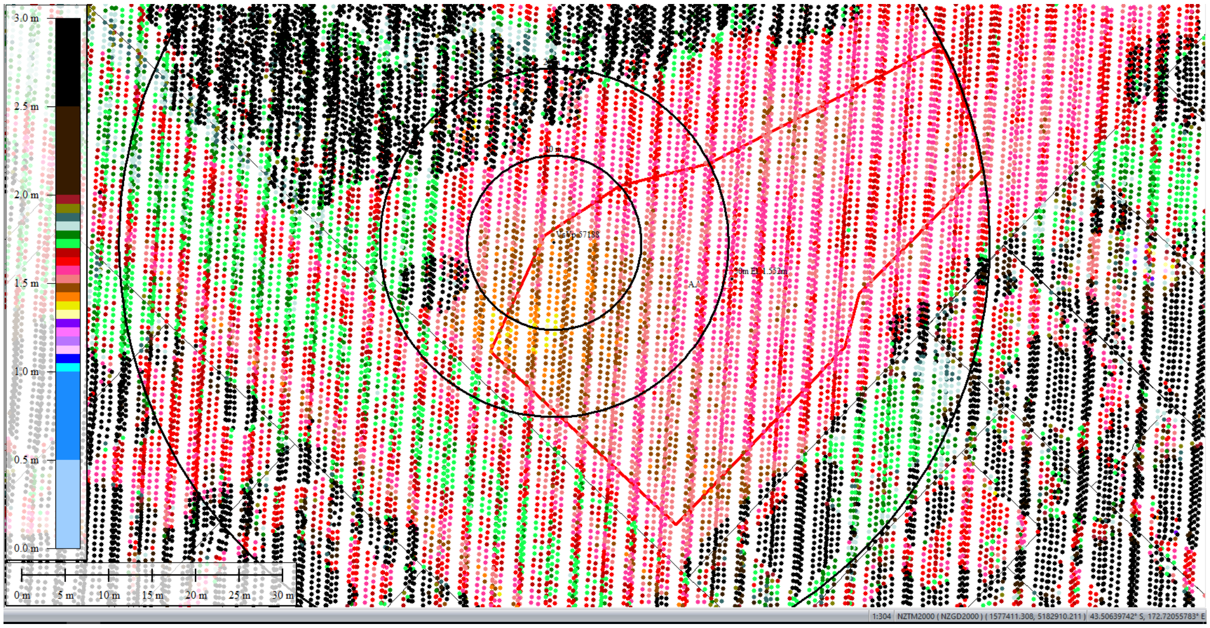


**Figure 47: Ground surface elevation averaged over 50-m buffer for Mar 2011 LiDAR survey.**

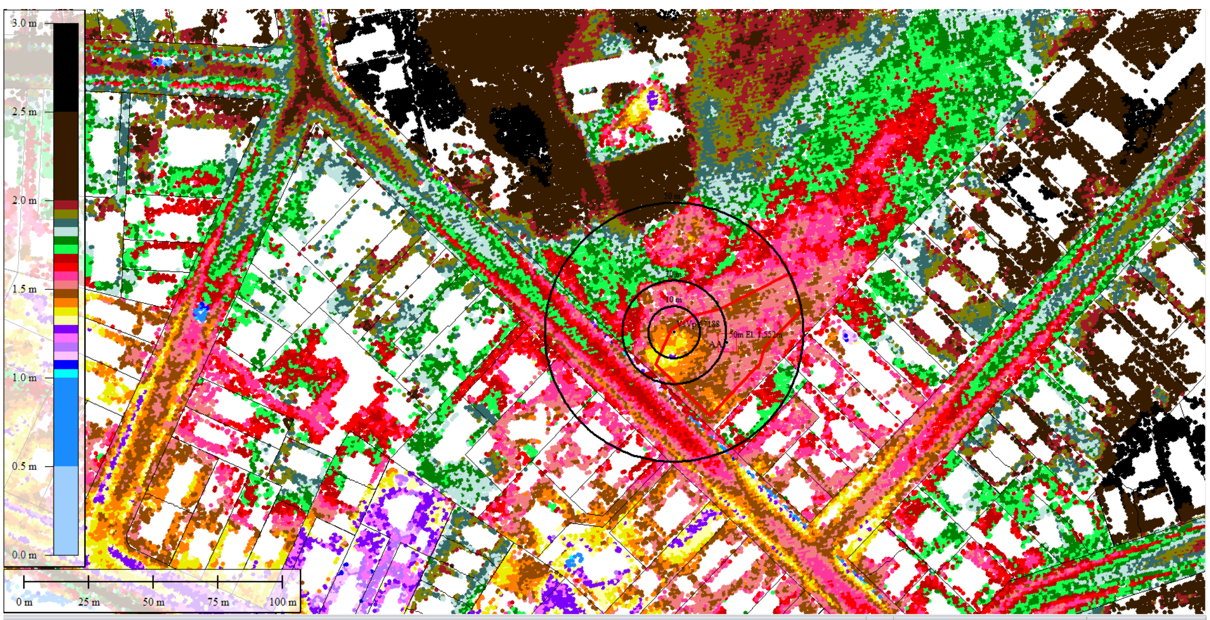


**Figure 48: May 2011 LiDAR survey.**

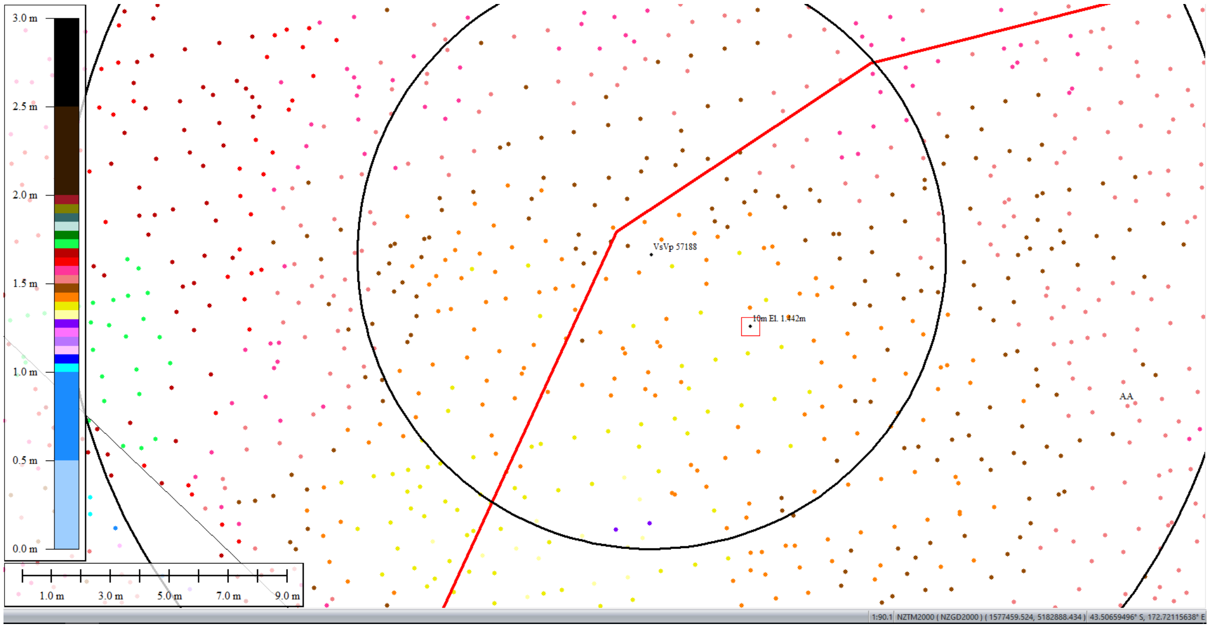

**Figure 49: Ground surface elevation averaged over 10-m buffer for May 2011 LiDAR survey.**

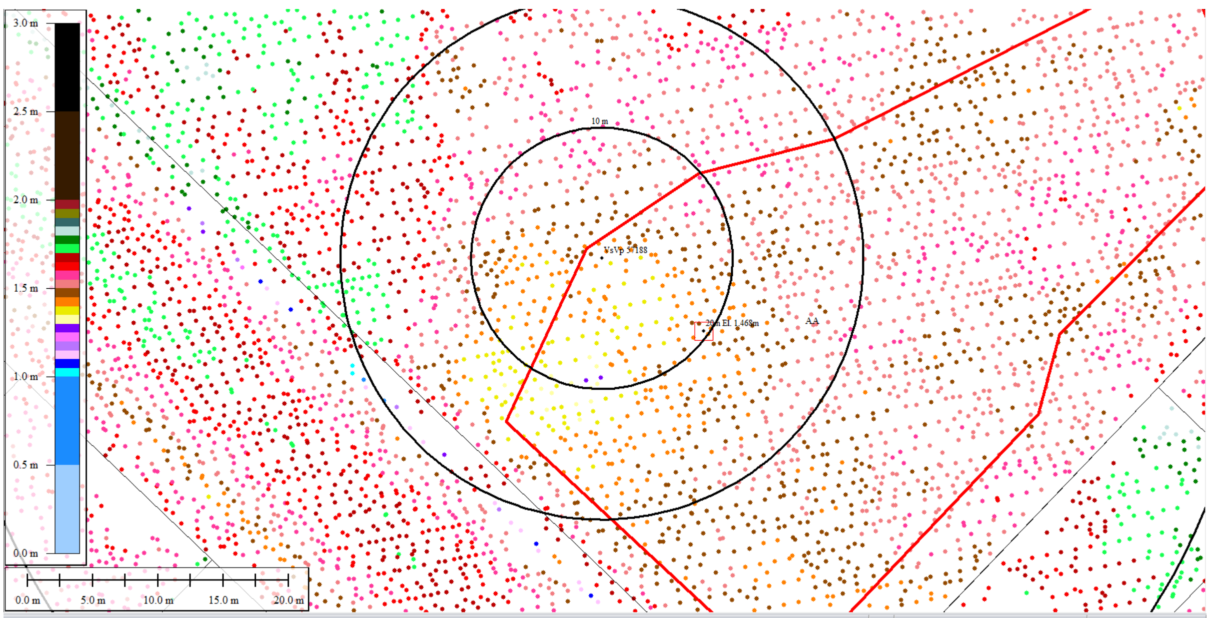

**Figure 50: Ground surface elevation averaged over 20-m buffer for May 2011 LiDAR survey.**

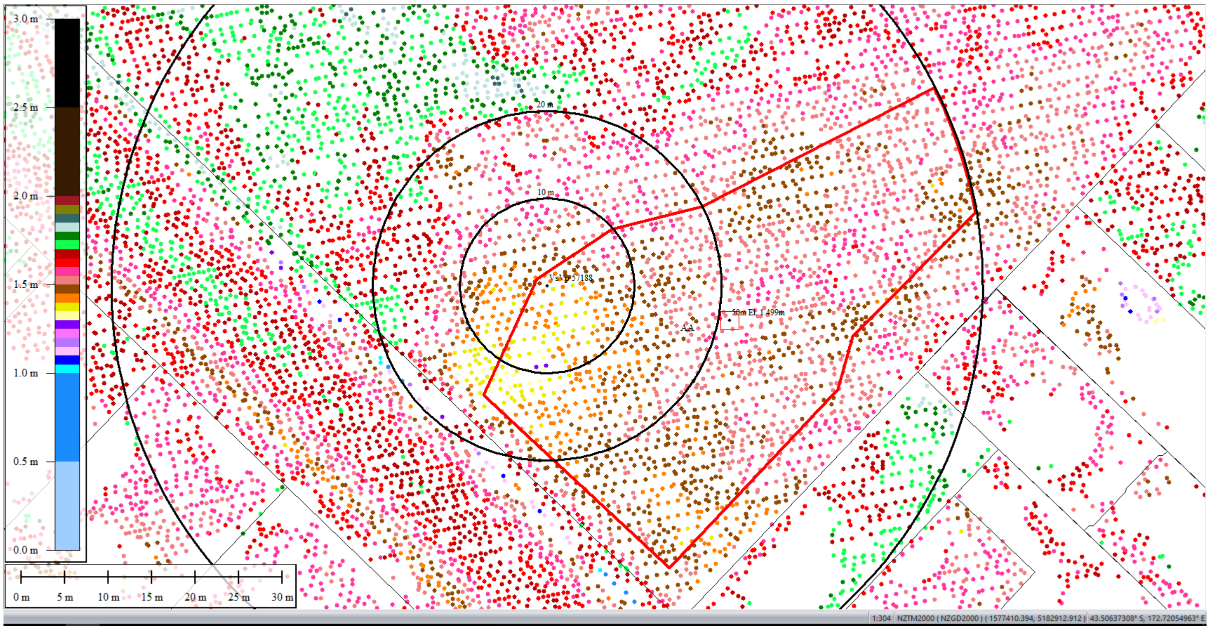

**Figure 51: Ground surface elevation averaged over 50-m buffer for May 2011 LiDAR survey.**

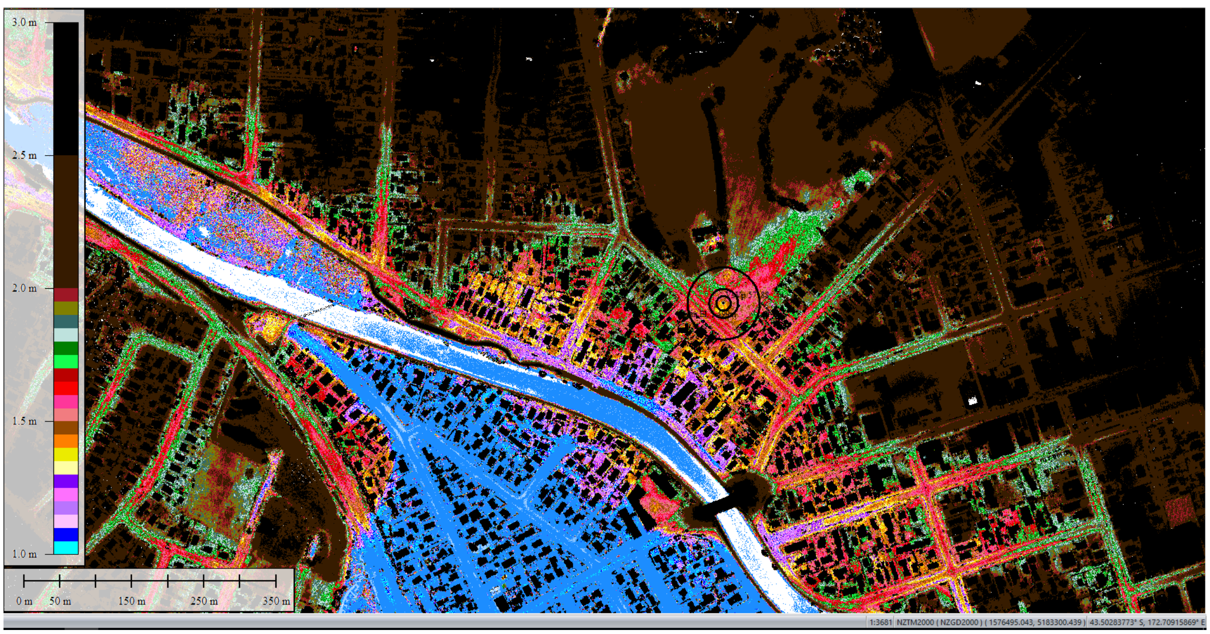

**Figure 52: Sep 2011 LiDAR survey.**

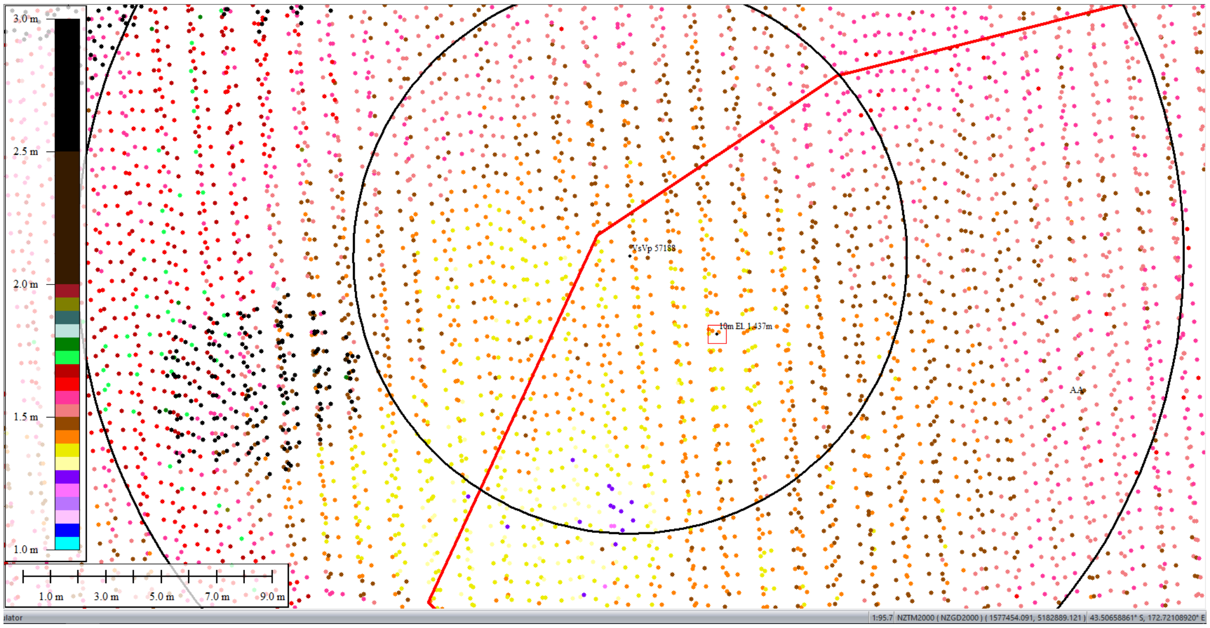


**Figure 53: Ground surface elevation averaged over 10-m buffer for Sep 2011 LiDAR survey.**

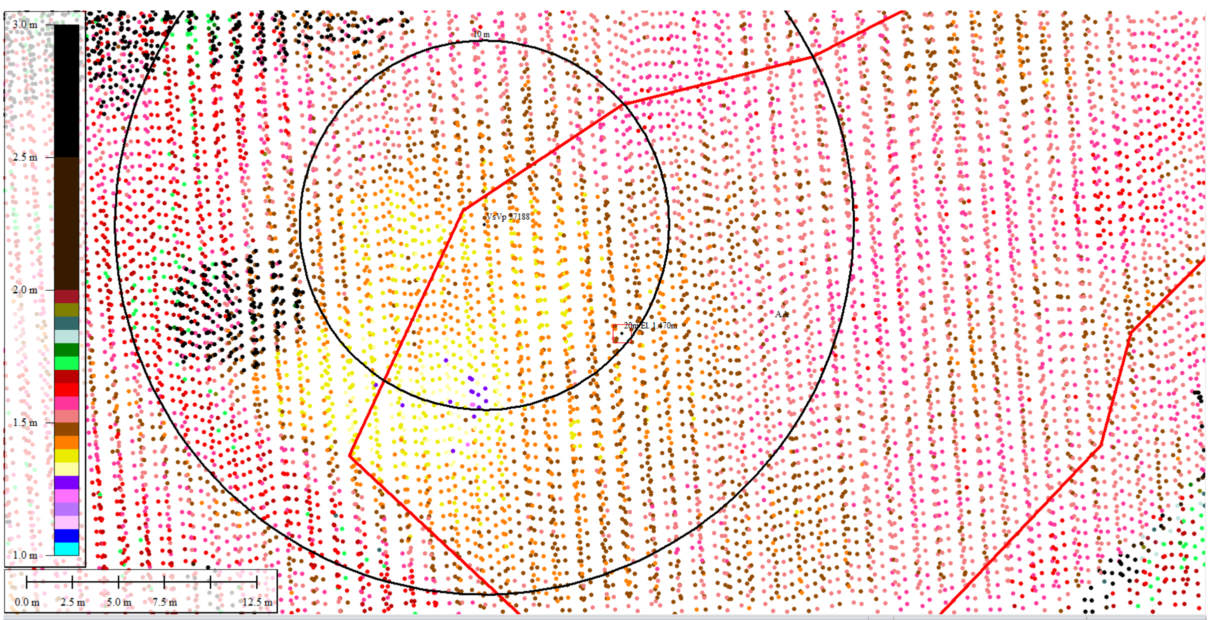


**Figure 54: Ground surface elevation averaged over 20-m buffer for Sep 2011 LiDAR survey.**

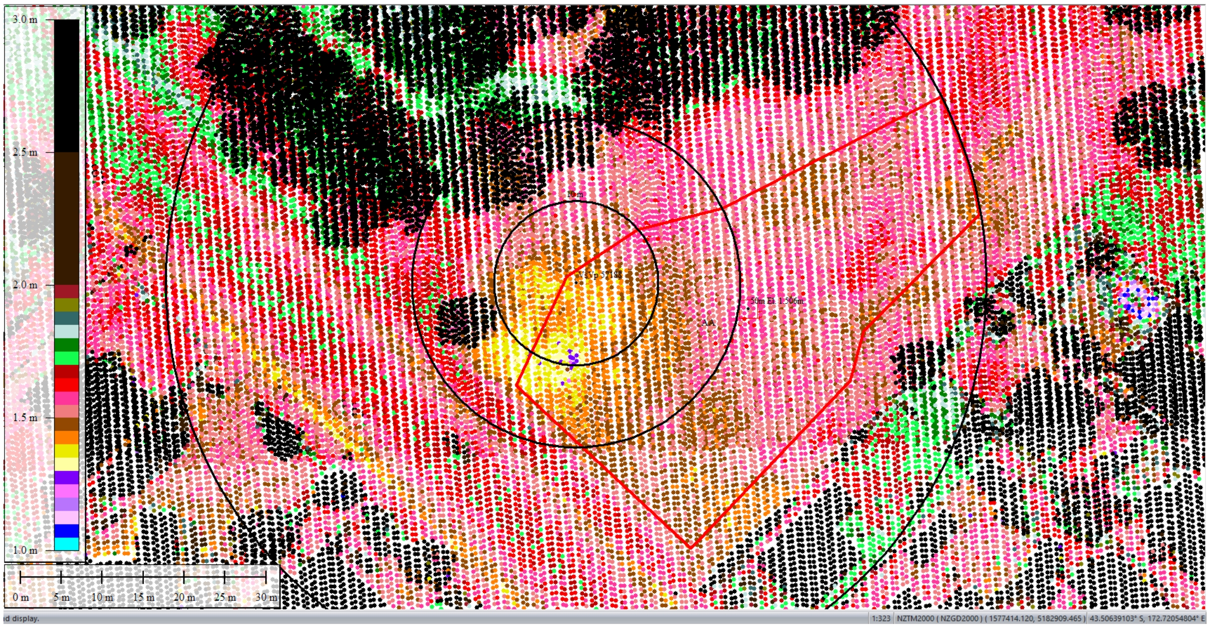

**Figure 55: Ground surface elevation averaged over 50-m buffer for Sep 2011 LiDAR survey.**

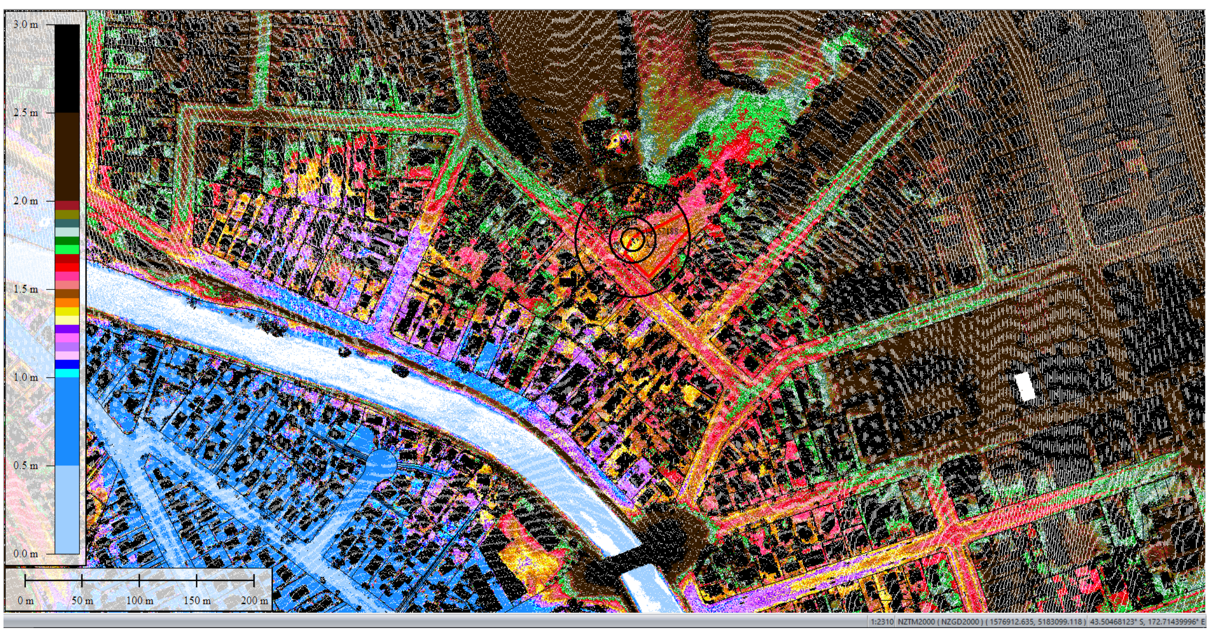

**Figure 56: Feb 2012 LiDAR survey.**

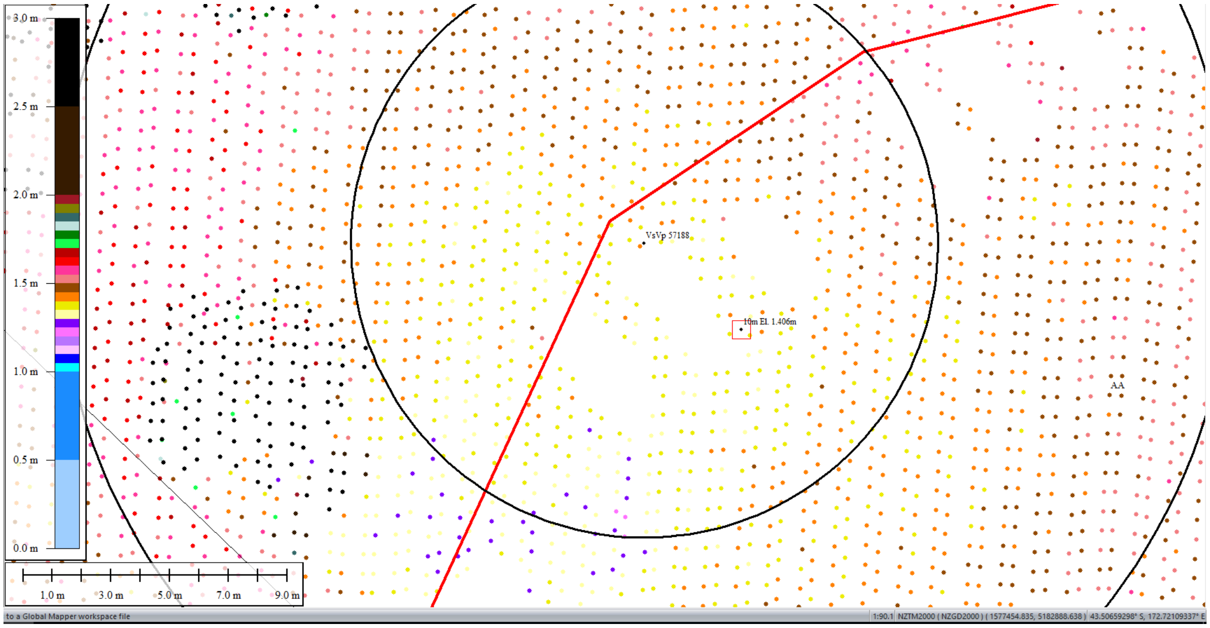


Figure 57: Ground surface elevation averaged over 10-m buffer for Feb 2012 LiDAR survey.

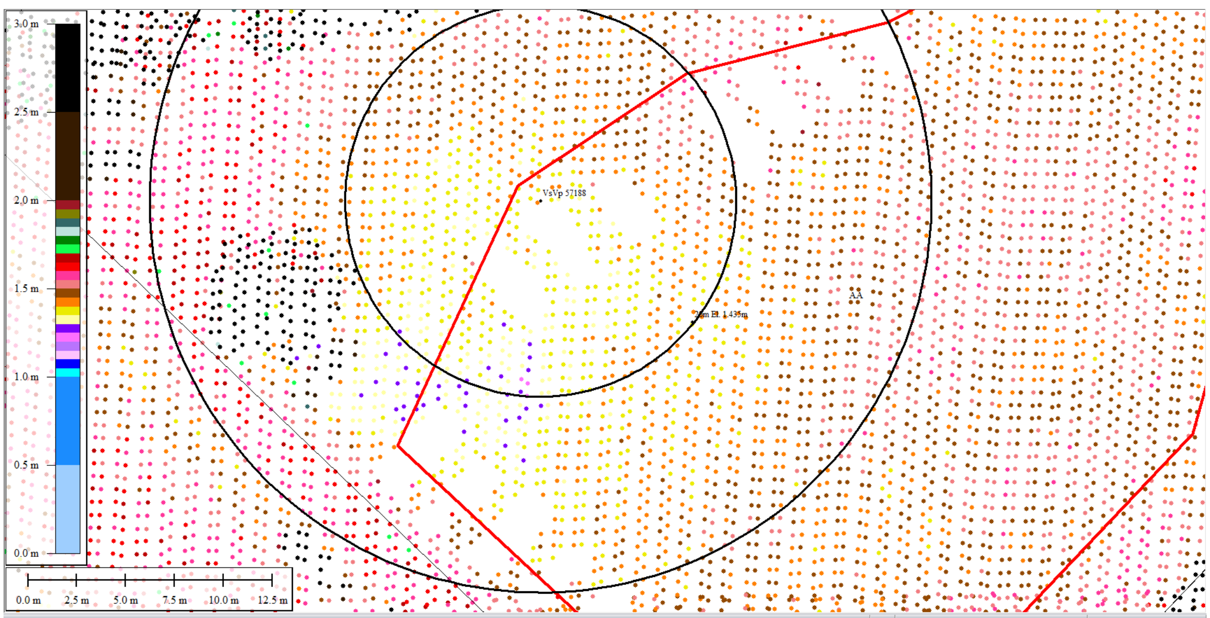


Figure 58: Ground surface elevation averaged over 20-m buffer for Feb 2012 LiDAR survey.

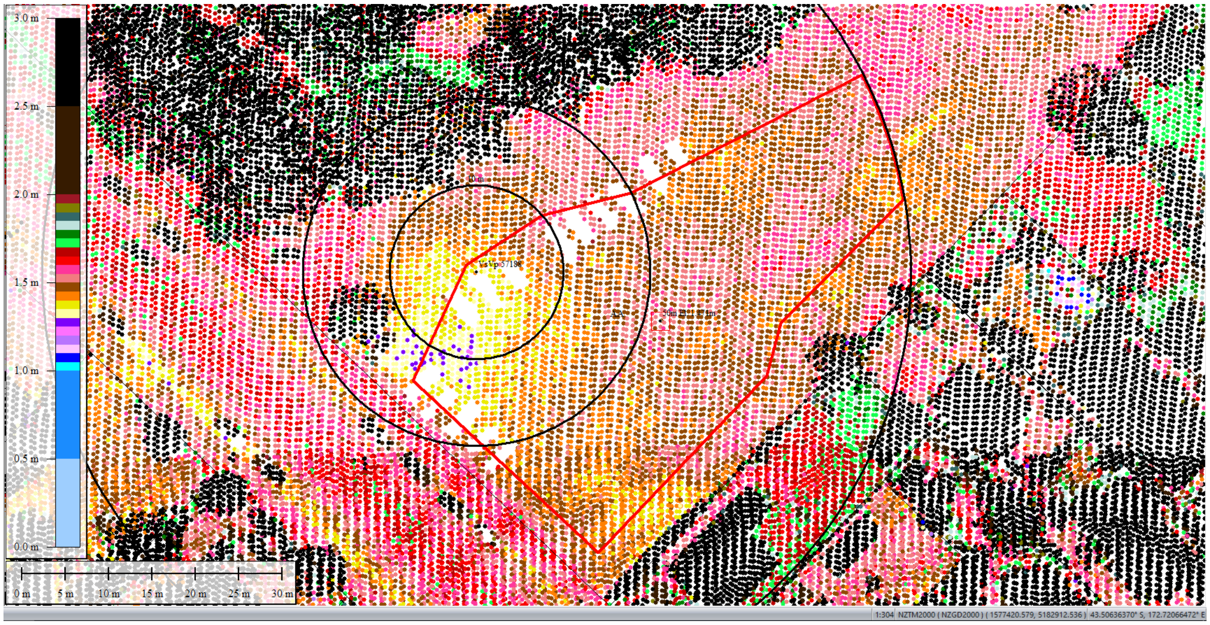


**Figure 59: Ground surface elevation averaged over 50-m buffer for Feb 2012 LiDAR survey.**

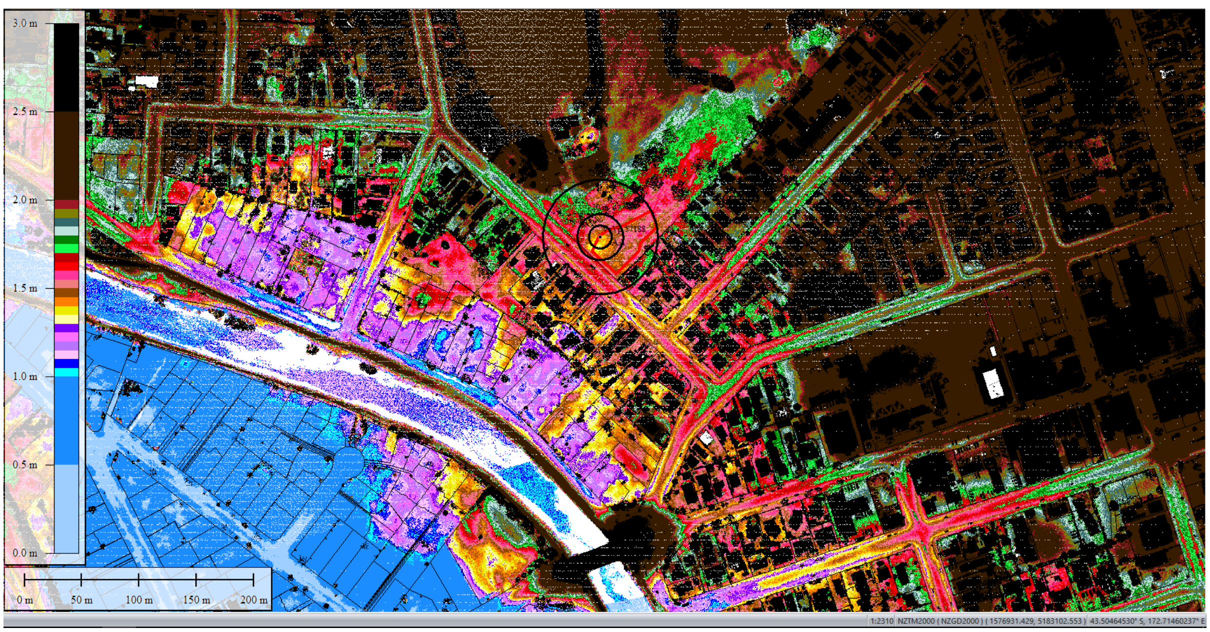


**Figure 60: Oct 2015 LiDAR survey.**

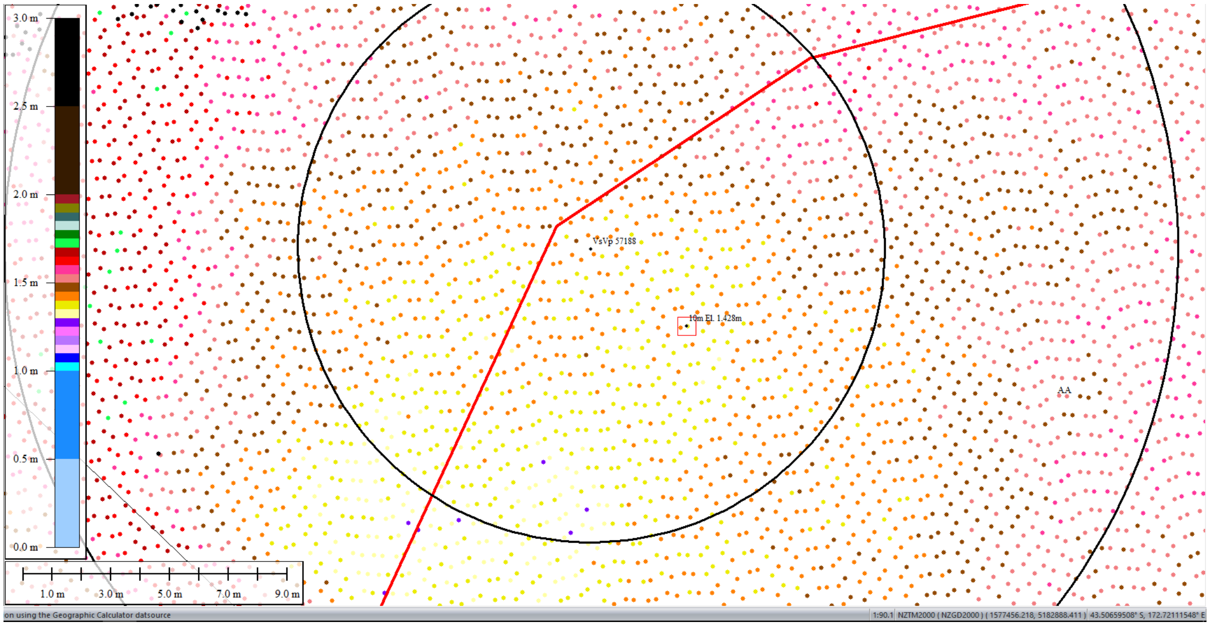

Figure 61: Ground surface elevation averaged over 10-m buffer for Oct 2015 LiDAR survey.

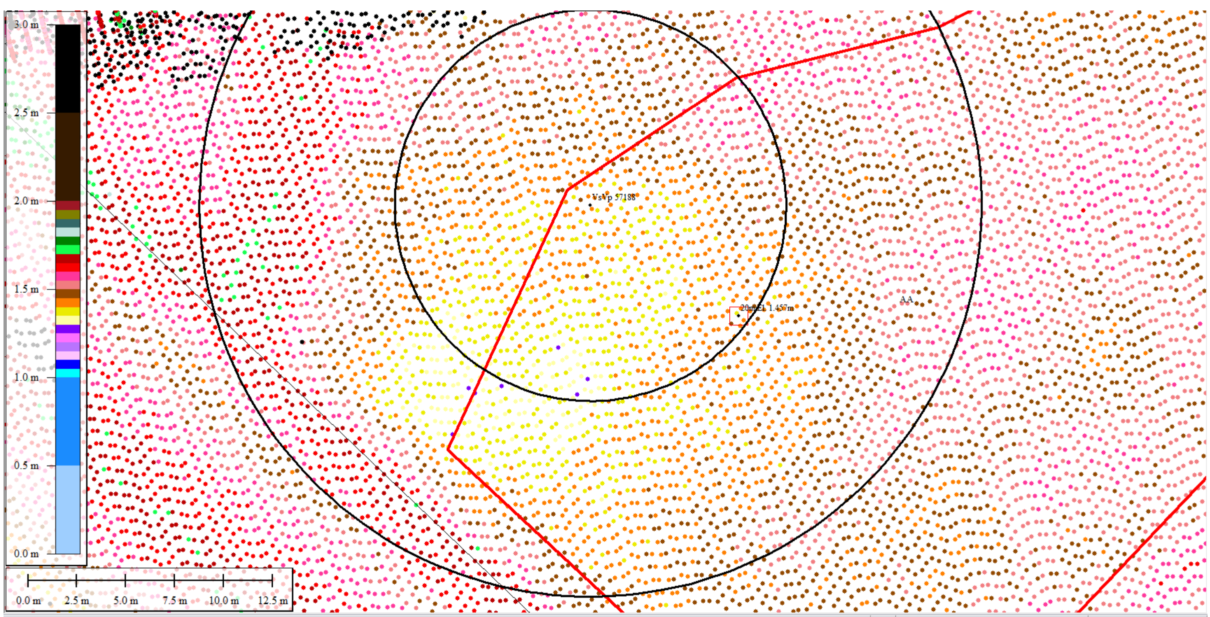

Figure 62: Ground surface elevation averaged over 20-m buffer for Oct 2015 LiDAR survey.

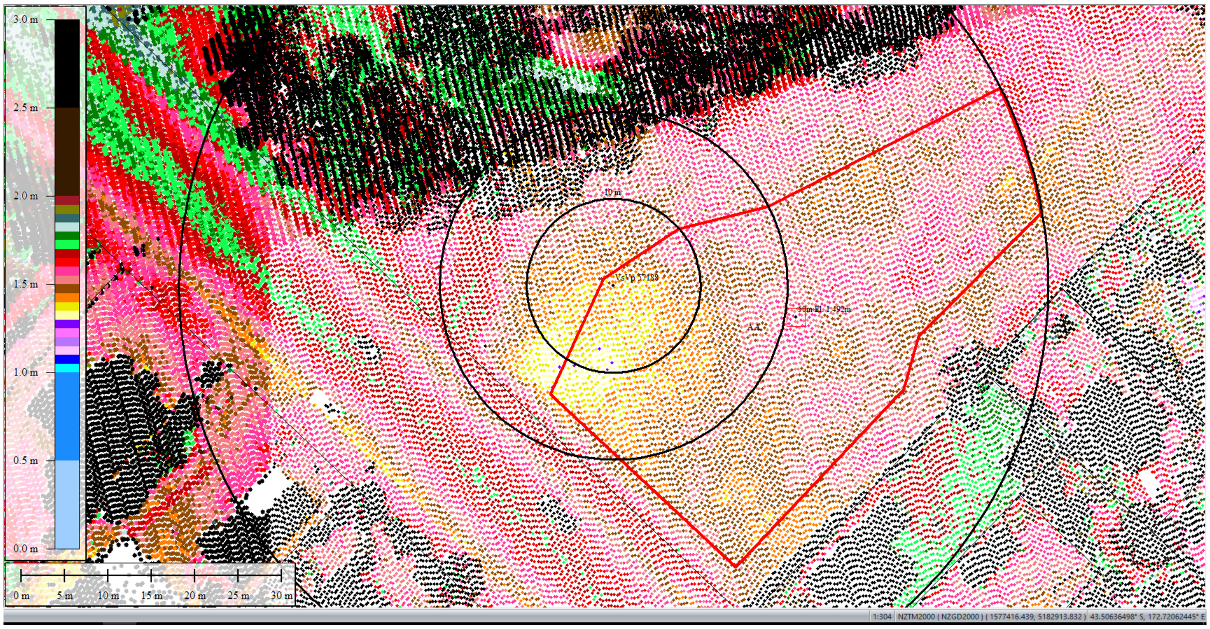


**Figure 63: Ground surface elevation averaged over 50-m buffer for Oct 2015 LiDAR survey.**


**Figure 64: Aerial photograph showing no ejecta at the site for Sep-10 EQ.**


**Figure 65: Aerial photograph showing no ejecta at the site for Feb-11 EQ.**


**Figure 66: Aerial photograph showing no ejecta at the site for Jun-11 EQ.**


**Figure 67: Aerial photograph showing no ejecta within the settlement assessment area for Dec-11 EQ. There are negligible ejecta on the road within the 50-m buffer.**


**Figure 68: CPT locations.**

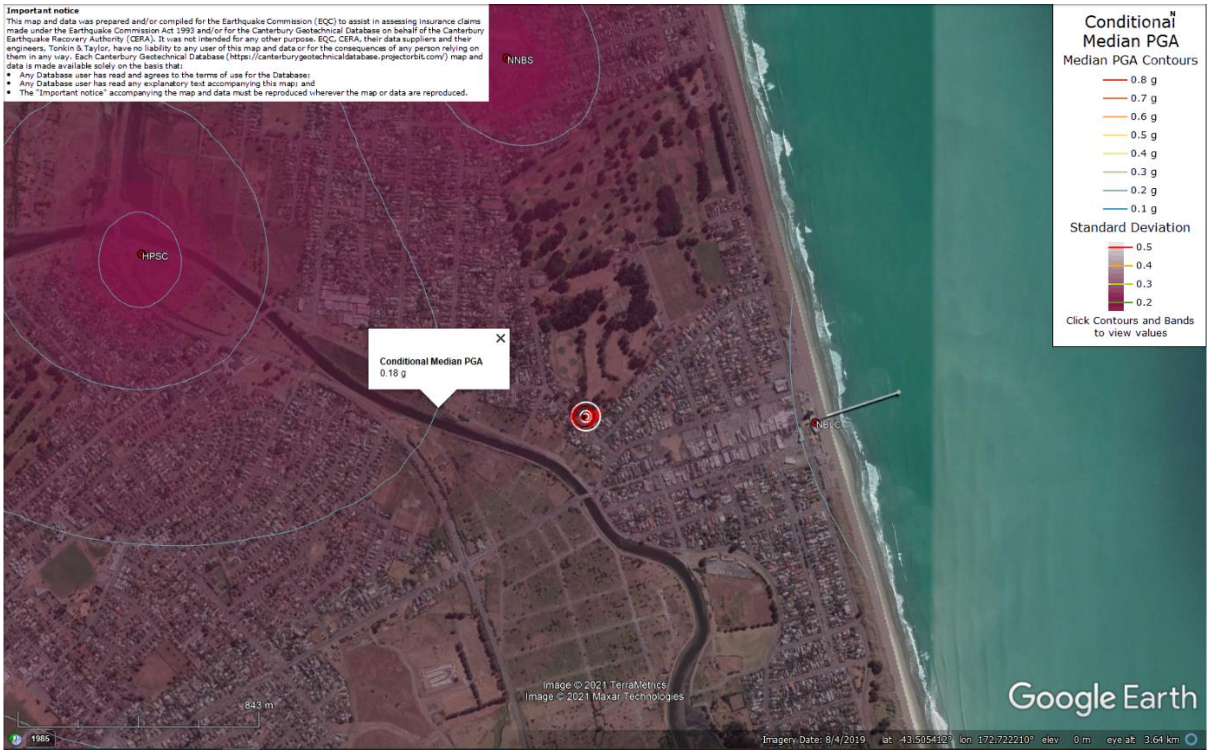


Figure 69: PGA for Sep-10 EQ (st. dev = 0.300-0.325 ln units).

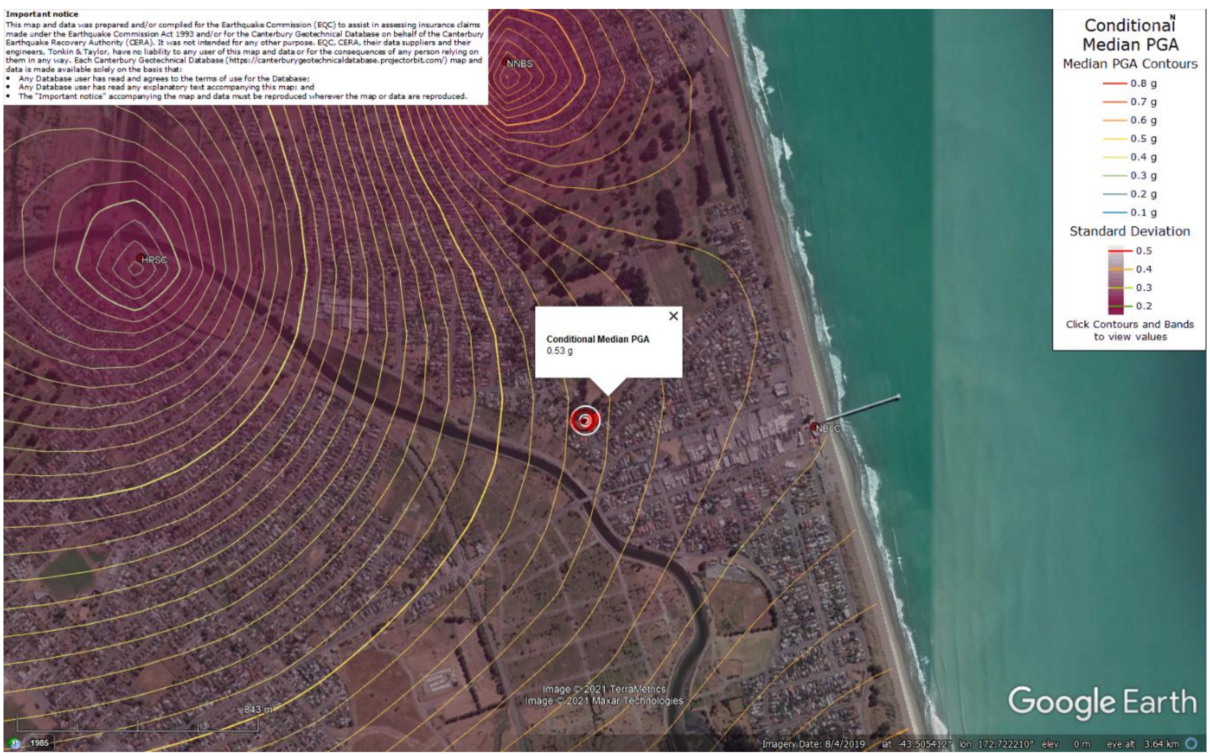


Figure 70: PGA for Feb-11 EQ (st. dev = 0.325-0.350 ln units).

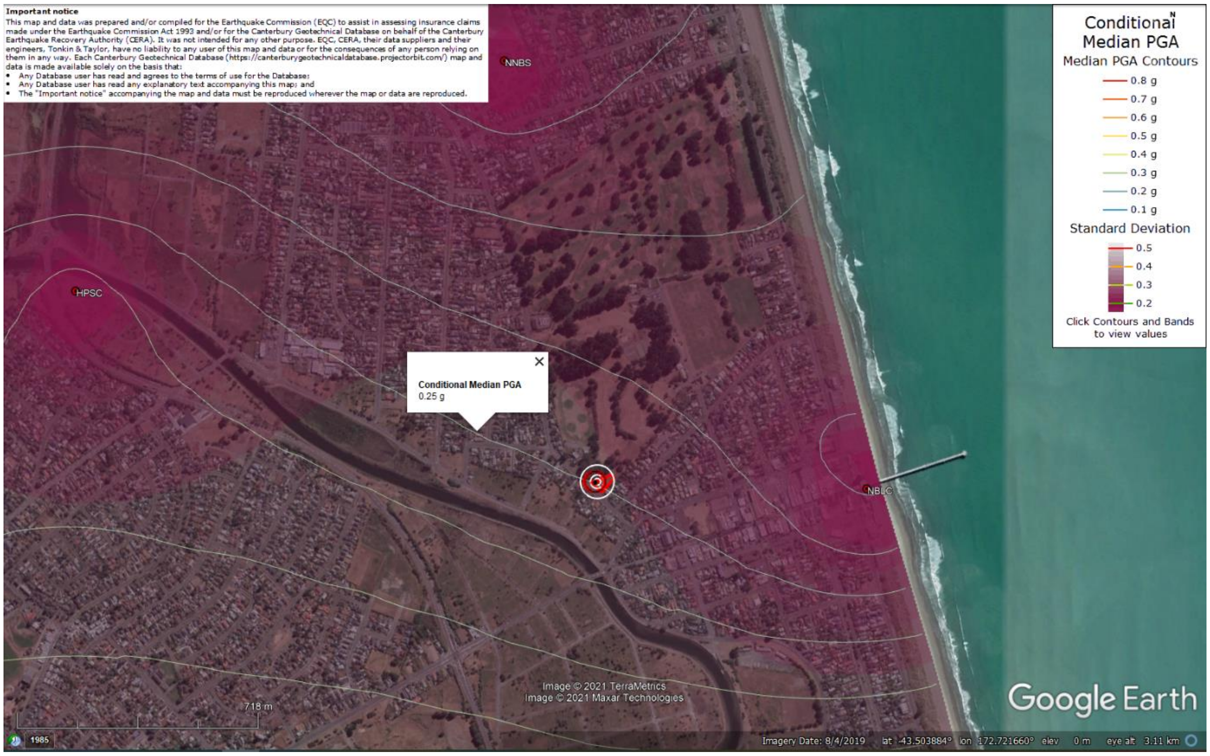


Figure 71: PGA for Jun-11 EQ (st. dev = 0.300-0.325 ln units).

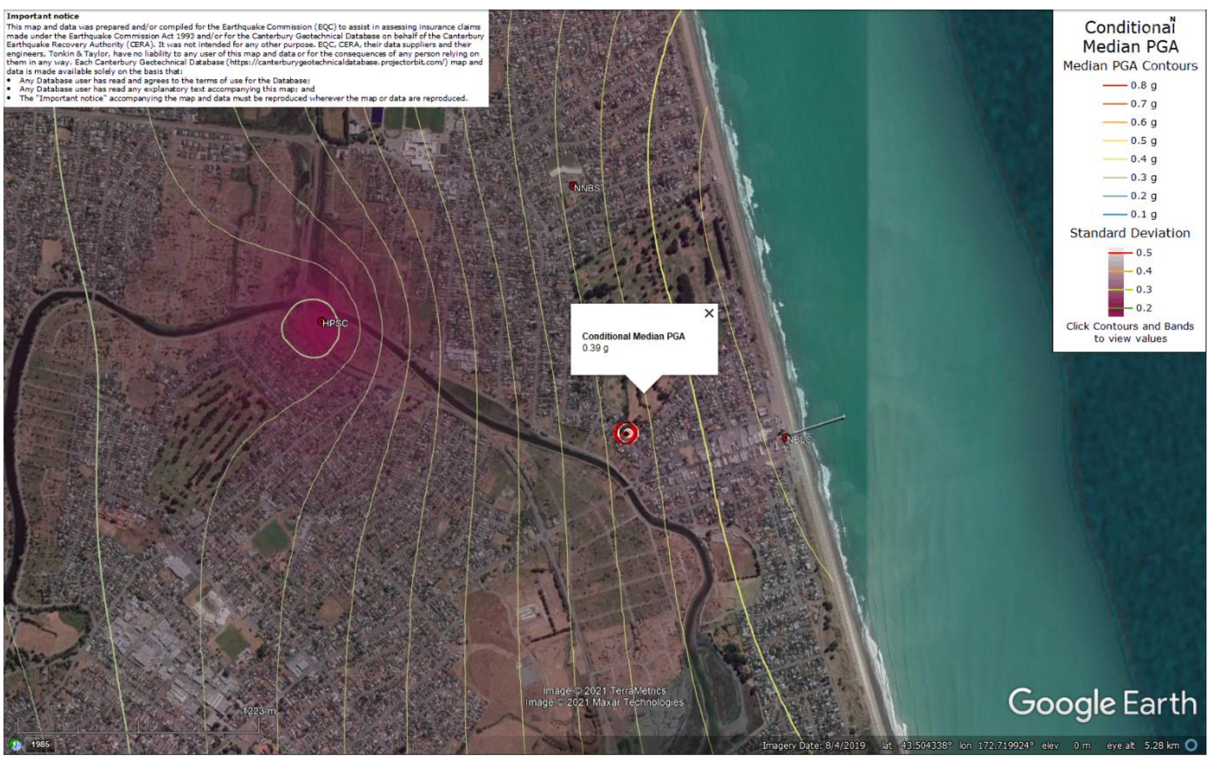


Figure 72: PGA for Dec-11 EQ (st. dev = 0.400-0.425 ln units).

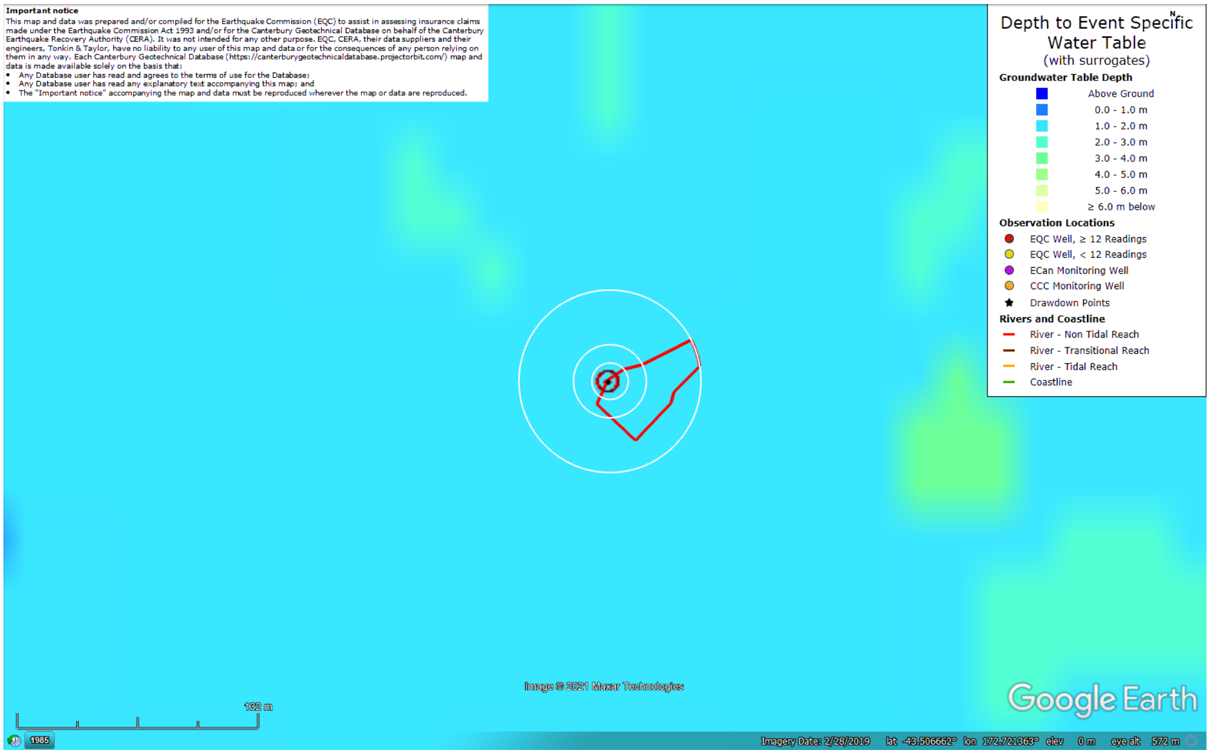


**Figure 73: Depth to groundwater table for Sep-10 EQ.**

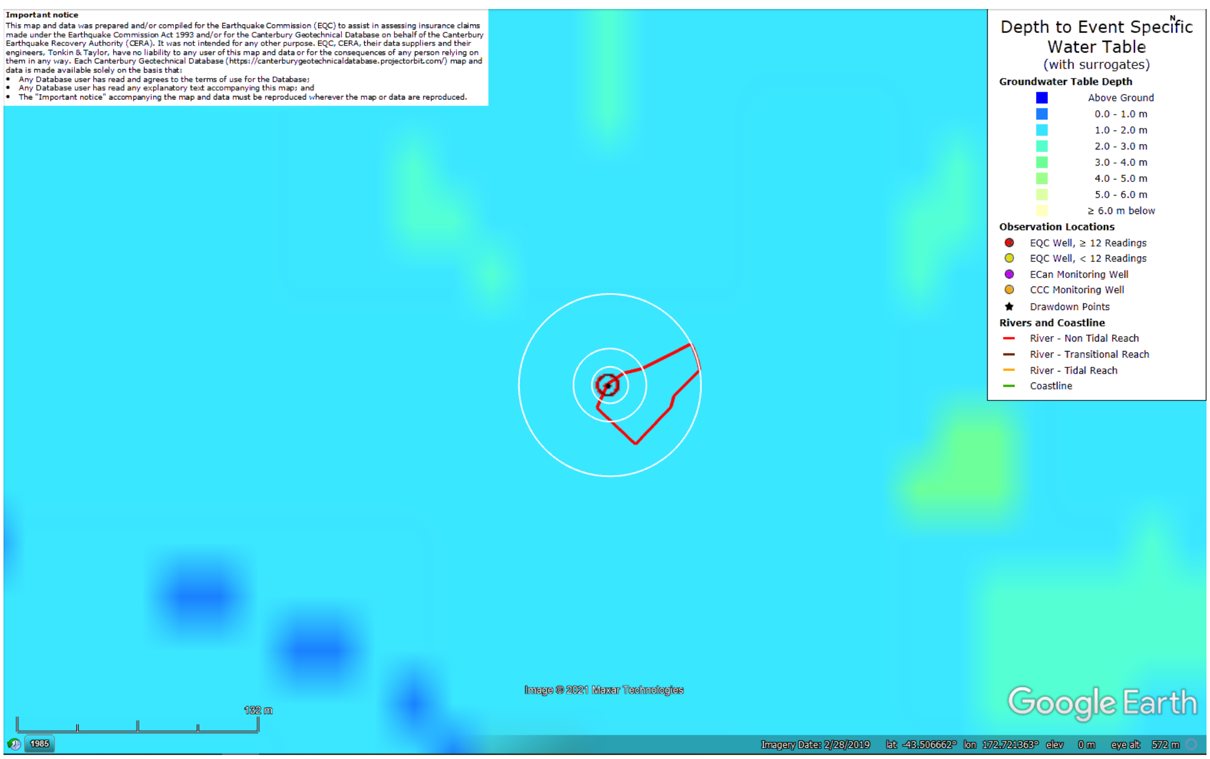


**Figure 74: Depth to groundwater table for Feb-11 EQ.**

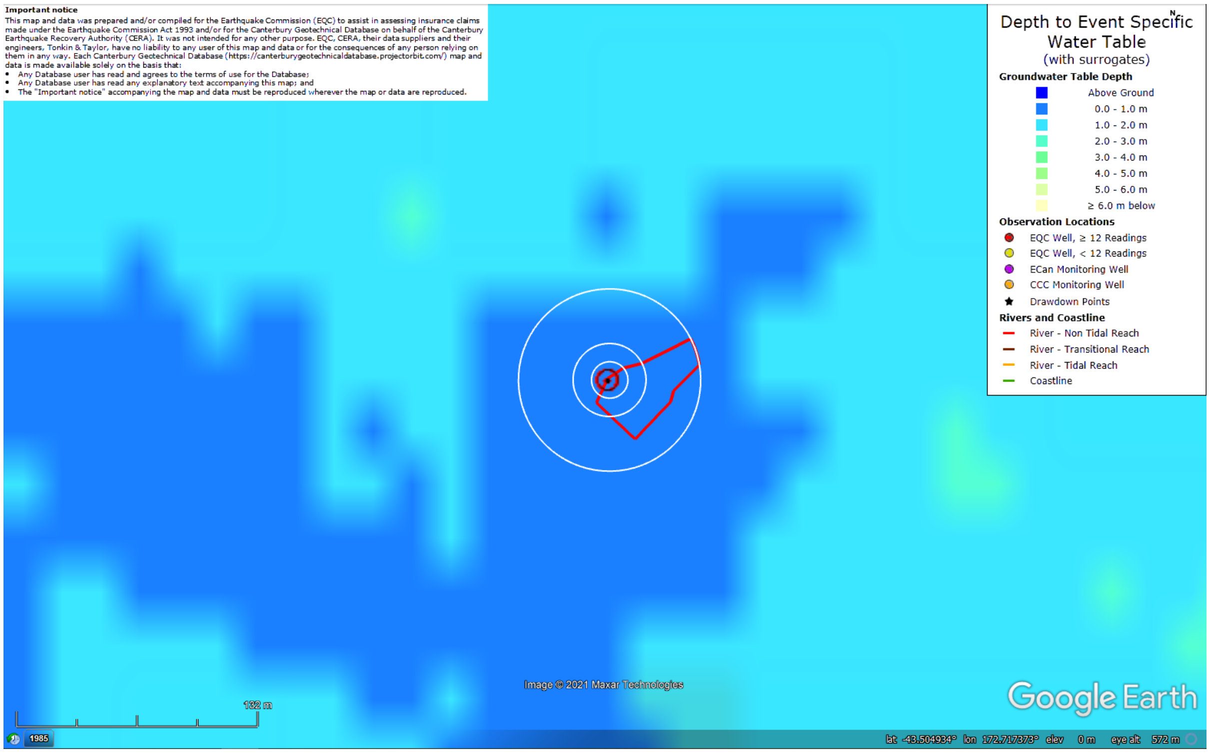


Figure 75: Depth to groundwater table for Jun-11 EQ.


Figure 76: Depth to groundwater table for Dec-11 EQ.

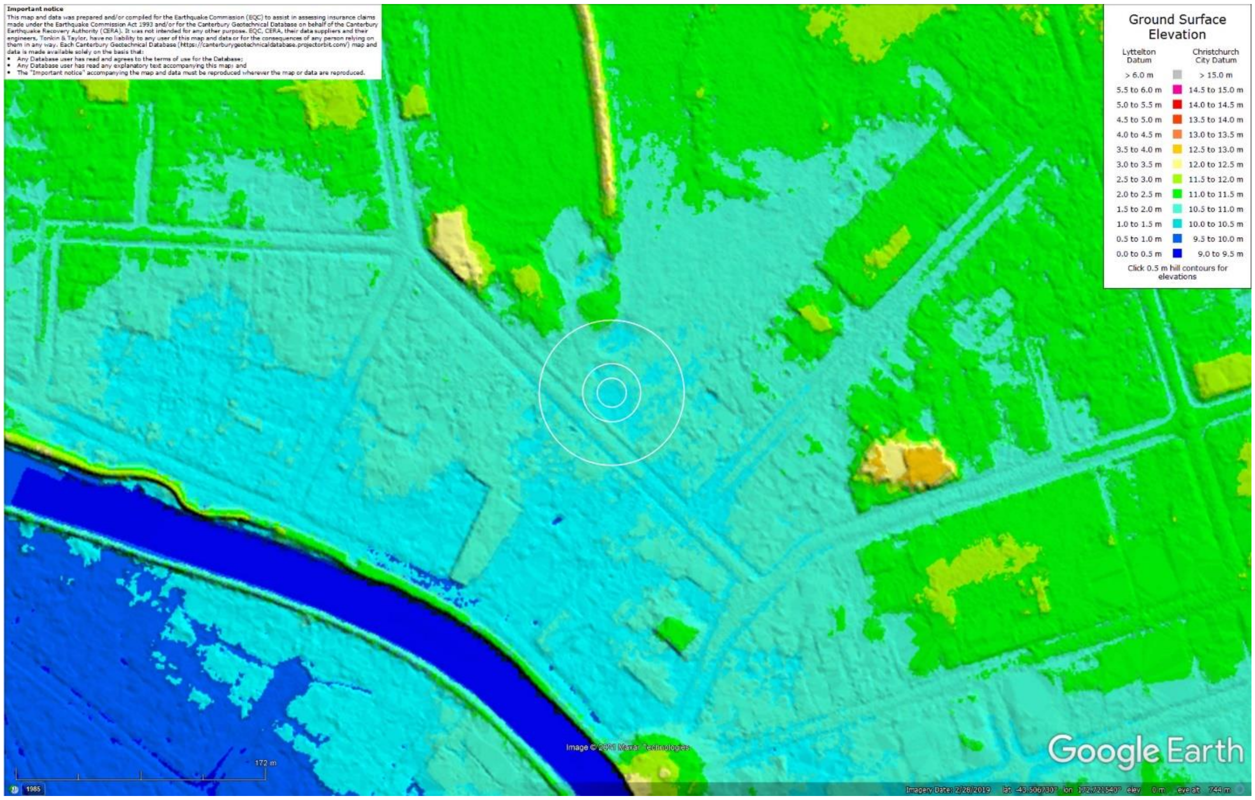


**Figure 77: Ground surface elevation according to the Sep-11 LiDAR survey.**

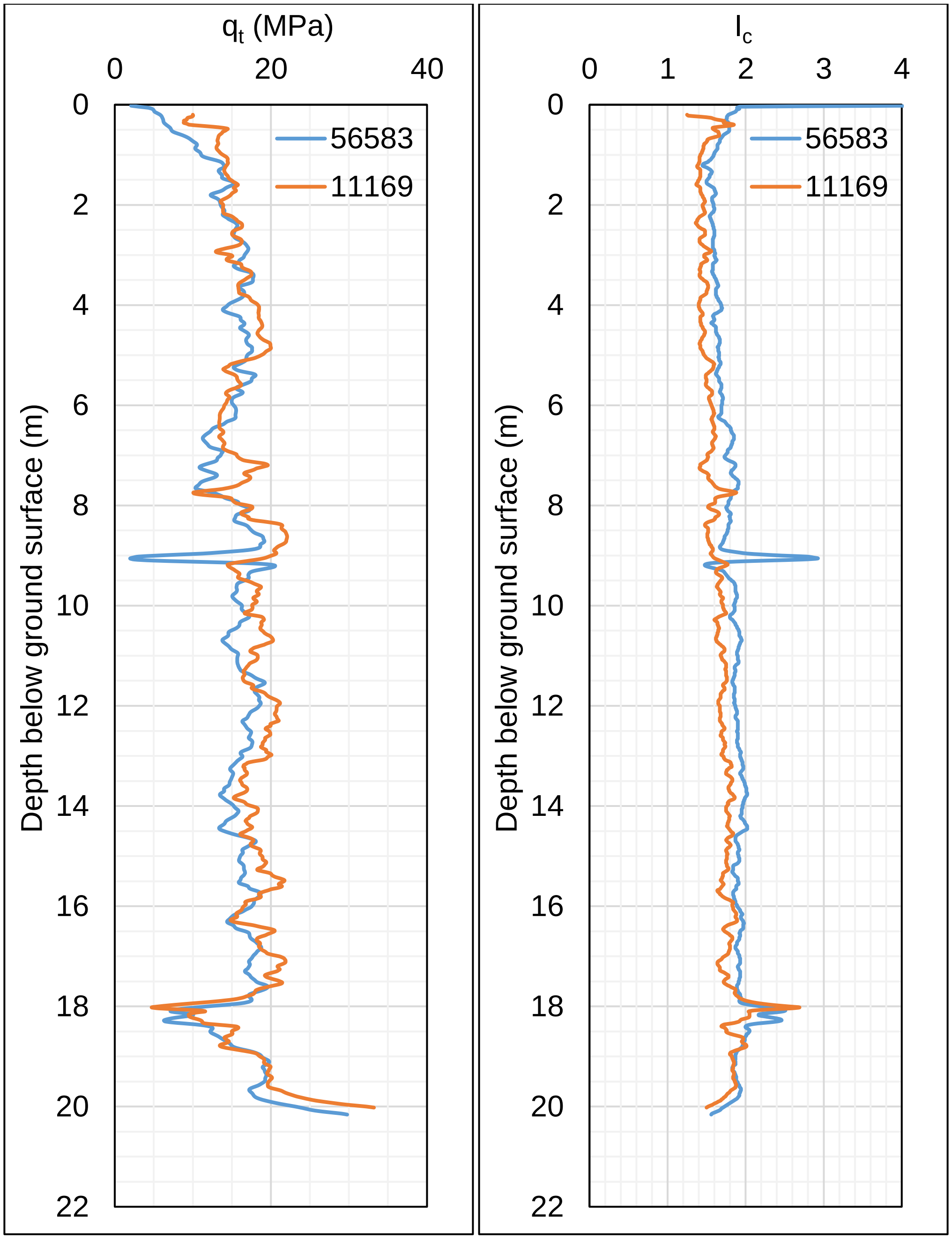


**Figure 78: $q_t$ and $I_c$ profiles.**

**Note 6:** The selection of CPTs for the area considered for settlement assessment (Figure 1) is based on the proximity of the CPTs to the considered areas. In accordance with that, the following table shows CPTs that were used for the volumetric settlement analysis in *Cliq v.3.0.3.2*, a CPT soil liquefaction software developed by GeoLogismiki. (The average volumetric settlements were reported in Table 8.)

**Table 12: CPT profiles used in volumetric settlement analysis for areas selected for settlement assessment.**

| CPT ID No. | 10-m buffer | 20-m buffer | 50-m buffer |
|---|---|---|---|
| 57343 (56583) | ✓ | ✓ | ✓ |
| 11169 | | | ✓ |

**Table 13: CPT-based results.**

| | | CPT ID | |
|---|---|---|---|
| EQ Event | Parameter | 57343 | 11169 |
| Sep-10 | $S_{V1D}$ (mm) | 1 | 1 |
| | LSN | 0 | 0 |
| | LPI | 0 | 0 |
| | $LPI_{ish}$ | 0 | 0 |
| | $D_{FS<1}$ (m) | undet. | undet. |
| Feb-11 | $S_{V1D}$ (mm) | 11 | 21 |
| | LSN | 1 | 2 |
| | LPI | 0 | 1 |
| | $LPI_{ish}$ | 0 | 0 |
| | $D_{FS<1}$ (m) | 18.02 | 6.16 |
| Jun-11 | $S_{V1D}$ (mm) | 2 | 2 |
| | LSN | 0 | 0 |
| | LPI | 0 | 0 |
| | $LPI_{ish}$ | 0 | 0 |
| | $D_{FS<1}$ (m) | undet. | undet. |
| Dec-11 | $S_{V1D}$ (mm) | 6 | 10 |
| | LSN | 0 | 1 |
| | LPI | 0 | 0 |
| | $LPI_{ish}$ | 0 | 0 |
| | $D_{FS<1}$ (m) | undet. | 18.14 |

Notes: $D_{FS<1}$ = Depth to the first liquefiable layer ($FS_L$<1) that is at least 200-mm thick, as determined by the Boulanger and Idriss (2016) liquefaction-triggering procedure ($P_L$=50%, $C_{FC}$=0.13, and $I_{c,cutoff}$ =2.6), and exported from *Cliq v.3.0.3.2*; undet. = the specified soil layer was not detected.

**Note 7:** Based on the borehole log (BH 57240, Figure 68), the groundwater table is at a depth of 1.1 m below the ground surface. The soil profile consists of poorly graded sand, SP, of the Christchurch formation to a depth of 11.05 m (the end of the borehole). The nearby borehole (BH 4411, ≈190 m away from the centre of the site) suggests the SP layer extends to a depth of 20 m. Trace angular, fine gravel is found from a depth of 0.2 m to a depth of 0.8 m.